약학박사 학위논문

Development of a novel iron oxide encapsulated prostate-specific membrane antigen (PSMA) targeting nanoparticle as a dual-modality imaging probe for PET and MRI

전립선특이막항원(PSMA) 표적화 PET과 MRI 이중영상용 신규 산화철 나노입자 프로브 개발

2016 년 8 월

서울대학교 대학원

협동과정 방사선응용생명과학전공

문 성 현

A Thesis of the Degree of Doctor of Philosophy

전립선특이막항원(PSMA) 표적화 PET과 MRI 이중영상용 신규 산화철 나노입자 프로브 개발

Development of a novel iron oxide encapsulated prostate-specific membrane antigen (PSMA) targeting nanoparticle as a dual-modality imaging probe for PET and MRI

August 2016

The Department of Interdisciplinary Program in Radiation Applied Life Science

Seoul National University

College of Medicine

Sung-Hyun Moon

전립선특이막항원(PSMA) 표적화 PET과 MRI 이중영상용 신규 산화철 나노입자 프로브 개발

지도교수 정 재 민

이 논문을 약학박사 학위논문으로 제출함

2016 년 4 월

서울대학교대학원

협동과정 방사선응용생명과학 전공

문 성 현

문성현의 약학박사 학위논문을 인준함

2016 년 8 월

위 원 장 _____ **(Seal)**

부위원장 _____ **(Seal)**

위 원 _____ **(Seal)**

위 원 _____ **(Seal)**

위 원 _____ **(Seal)**

Development of a novel iron oxide encapsulated prostate-specific membrane antigen (PSMA) targeting nanoparticle as a dual-modality imaging probe for PET and MRI

by
Sung-Hyun Moon

A thesis submitted to the Interdisciplinary Program in Radiation Applied Life Science in partial fulfillment of the requirements for the Degree of Doctor of Philosophy in Radiation Applied Life Science at Seoul National University College of Medicine

August 2016

Approved by Thesis Committee:

Professor _____ Chairman

Professor _____ Vice Chairman

Professor _____

Professor _____

Professor _____

ABSTRACT

SUNG-HYUN MOON

Department of Nuclear Medicine

Interdisciplinary Program in Radiation Applied Life Science

The Graduate School

Seoul National University College of Medicine

I tried to develop a multi-modality imaging probe for PET, MRI and PET/MR by encapsulation with specific amphiphiles using the original one-pot method developed by our study group. In this study, iron oxide (IO) nanoparticles were encapsulated with three amphiphiles containing PEG, DOTA and the prostate-specific membrane antigen (PSMA)-targeting ligand in aqueous medium. The diameter of the prepared nanoparticle DOTA-IO-GUL was 11.01 ± 1.54 nm. DOTA-IO-GUL was labeled with ^{68}Ga in high efficiency. The DOTA-IO-GUL showed a dose-dependent binding to 22Rv1 (PSMA positive) cells via a competitive binding study against ^{125}I-labeled MIP-1072 (PSMA-targeting agent). Additionally, PET and MR imaging results showed PSMA selective uptake by only 22Rv1 (PSMA positive) but not PC-3 (PSMA negative) in dual-tumor xenograft mouse model study. MR imaging showed high resolution, and PET imaging enabled quantification and confirmation of

the specificity. In conclusion, I have developed the specific PSMA-targeting IO nanoparticle, DOTA-IO-GUL, as a multi-modality probe for complementary PET, MRI and PET/MR imaging. Additionally I could confirm the reproducibility and scalability of the original one-pot method.

Keywords: Nanoparticle; encapsulation; original one-pot method; Iron Oxide; PET; MRI; PET/MR; prostate cancer; multi-modal

Student Number: 2011-30624

CONTENTS

LIST of FIGURES and TABLES

LIST of SCHEMES

LIST of ABBREVIATIONS

PSMA	Prostate Specific Membrane Antigen
IO	Iron Oxide
NPs	Nanoparticles
PEG	Polyethylene glycol
DOTA	1,4,7,10-Tetraazacyclododecane-1,4,7,10-tetrakis (acetamido methylenephosphonic acid)
GUL	Glutamate-Urea-Lysine
DOTA-SA	2,2',2",2"'-(2-(4-(3-octadecylthioureido)benzyl)-1,4,7,10-tetraazacyclododecane-1,4,7,10-tetrayl)tetraacetic acid
GUL-SA	(S)-2-(3-((S)-1-carboxy-5-stearamidopentyl) ureido) pentanedioic acid
DOTA-IO-GUL	Iron Oxide nanoparticle encapsulated with DOTA-SA and GUL-SA
NOTA-SCN-GUL	(2S)-2-(3-((1S)-1-carboxy-5-(3-(4-((1,4,7-tris(carboxymethyl)-1,4,7-triazonan-2-yl)methyl)phenyl)thioureido)pentyl)ureido)pentanedioic acid
PET/CT	Positron Emission Tomography/Computed Tomography
MRI	Magnetic Resonance Imaging
PET/MR	Positron Emission Tomography/Magnetic Resonance Imaging
DLS	Dynamic Light Scattering

TEM	Transmission Electron Microscopy
AAALAC	Association for Assessment and Accreditation of Laboratory Animal Care International
ATCC	American Type Culture Collection

INTODUCTION

Prostate cancer is one of the most common types of cancer in men worldwide (*1, 2*). Especially the prostate cancer is the highest cancer in North America, and the second highest reason of death in men (*3*). And also in Korea, the prostate cancer has become the 5th common cancer in 2012 and rapidly increase (*4*).

Prostate Specific Antigen (PSA) detection is most common diagnosis method of prostate cancer. However, PSA could be detected not only prostate cancer but also prostatic hyperplasia, prostatitis and etc (*5*). The prostate-specific membrane antigen (PSMA) can be another alternative biomarker to targeting prostate cancer (*6*).

PSMA is a type II membrane glycoprotein consisting of a small intracellular segment of 18 amino acids, which is a well-known biomarker of prostate cancer. PSMA has enzymatic activity of folate hydrolase and N-acetyl-alpha-linked acidic dipeptidase (NAALADase). The PSMA is the transmembrane domain and an extensive extracellular domain that contains the catalytic site. Many study groups, which are development about prostate cancer development and diagnosis, are focused to PSMA targeting molecules (*6-11*). Furthermore, the glutamate-urea-lysine (GUL) conjugate has been proven to be a PSMA targeting moiety and its 3D structure has also already been published (*12*). Unlike several years study about PSMA role in prostate cancer, the role is still

unknown. In a recently published PSMA review article, they suggested that future study of PSMA will focus on its intracellular functions (*13*).

Many of developed PSMA targeting drug and drug-like agents are small molecule type. This compounds can be produced by organic synthesis, and introduced many kinds of chelator for an introduction of an radioisotope. And fluorescence imaging moiety also introduced. However, this kind of chemical compounds has shown the same drawback such as a high kidney uptake (*14*).

Nanoparticles (NP) are widely studied for their use as imaging probes (*15, 16*), especially because, they have a large surface area relative to volume or diameter, which allows them to introduce special ligands and multiple beacons for targeting and imaging (*17, 18*). Various surface modification methods have been investigated to produce multimodal imaging NPs, most of which included step-by-step modification using chemical reactions and purification. However, these methods have intrinsic drawbacks such as low yield and poor reproducibility (*19, 20*). A novel one-pot encapsulation method producing high yield and reproducibility has been reported (*21-24*) in this method, NPs are mixed and encapsulated with specially designed amphiphiles by vortexing, heating, and sonication. This method could easily be applied to various kinds of NPs with a hydrophobic surfaces, such as quantum dots, iron oxide, gold and etc (**Table 1**).

Positron Emission Tomography (PET) is a nuclear imaging modality, which is steadily used in clinical study nowadays. The PET has used a positron emitter, which is shown a high sensitivity. It can be shown functional

differences in molecular levels using radiopharmaceuticals specific target to organs and diseases, especially tumors. It can be also possible to detect the non-invasive imaging about the molecular events in the human body. However, the PET cannot show an exact anatomical data (**Figure 1**).

In contrast, Magnetic Resonance Imaging (MRI) tools can be detected with high-resolution anatomic data. The MRI is a major molecular imaging tools in radiology. Nevertheless, a low sensitivity and using high-dose contrast agents are challengeable issues in MRI contrast agent study groups (*25*).

A combined system of PET and MRI dual-imaging emerged as an important topic in nuclear medicine and molecular imaging studies (*26-31*). PET/computed tomography (CT) was developed for its complementary effect of using both PET and CT imaging, which replaced most PET-only instruments. Because of the higher sensitivity and specificity of MR imaging compared with CT, PET/MR dual-imaging is expected to be the next generation of PET/CT (*32-37*). Thus, the development of a probe for PET/MR dual-imaging is necessary for the implementation of this synergistic instrument. Especially recent study of PET/MRI agents are used many of metals which are Gd, Cu, Zr and iron oxide and etc (*38-42*). These PET/MRI agents used in T1 or T2 MR imaging due to each metals have different functions and characters.

^{68}Ga is a well-known positron emitter having an adequate half-life for diagnostic imaging (68 min), and is produced by a ^{68}Ge/^{68}Ga-generator which has huge economical and technical merits (*43, 44*). Bifunctional chelating agents are essential for labeling NPs with ^{68}Ga.(*45-47*) The 1,4,7,10-

tetraazacyclododecane-1,4,7,10-tetraacetic acid (DOTA) is one of the most widely used bifunctional chelating agents (*48*).

Iron oxide (IO) NPs have been actively investigated as MRI contrast agents in clinical trials (*49-54*). Furthermore, they have also been applied as PET/MR dual imaging probes after being labeled with positron emitters (*22, 34, 37, 55*).

Particularly, DOTA could be used for both diagnostic radioisotopes such as ^{68}Ga and ^{111}In, and therapeutic radioisotopes such as ^{90}Y and ^{177}Lu, which is important for the theragnostic use of NPs.

In this study, I aim to develop a new PSMA-targeting IO NP for use in PET, MRI, and PET/MR multimodality imaging probe. To achieve this, I employed the encapsulation method using amphiphiles containing DOTA and GUL each conjugated with a long alkyl chain and commercially available IO NP. The DOTA moiety was used for labeling with ^{68}Ga and the GUL moiety was used for targeting PSMA. The IO core was used for MR imaging. In addition, the developed nanoparticle was compared with PSMA targeting small molecule due to make clear the points about advantages and disadvantages From the development of PSMA targeting nanoparticle by the original one-pot method of our group I could prove that the reproducibility and the scalability of the method.

Table 1. NANOPARTICLE ENCAPSULATIO NMETHOD

	Known Method	Original one-pot Method developed by our lab
Synthetic method	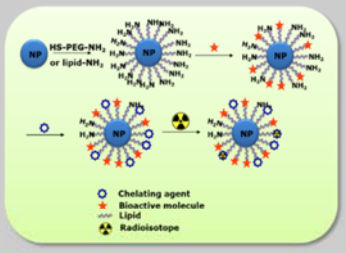	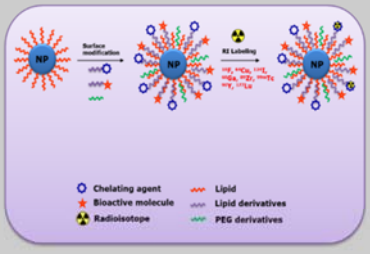
Preparation	No need	Synthesized functional moiety compounds
Reaction Step	Multi step	Single step
Yield	Low	High
Reproducibility	NOT good	Good
Scalability	Hard	Easy

A known method of nanoparticle encapsulation; This method has advantage about no need any other synthetic compounds. However, step by step method for functionalized group introduction can be one of disadvantage. And low reproducibility and scalability are disadvantages neither.

In contrast, Original one-pot method was developed from our study group. This critical method should prepare synthesized compounds, however after that it can be used only one pot reaction for functionalized group introduction. This method can be shown high reproducibility and scalability.

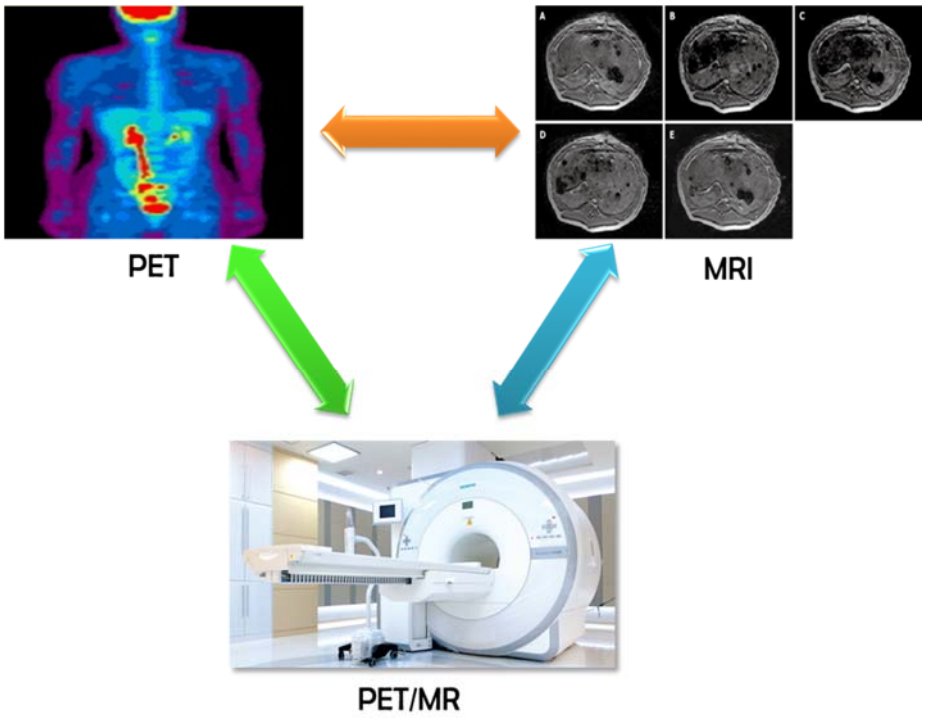

Figure 1. Clinical imaging tools.

PET is nuclear medicinal imaging tool used by radio isotope which can be shown a high sensitivity as a major advantage; MRI is molecular imaging tool using with metal contrast agents. High resolution is a major advantage.; PET/MR is merged imaging tool of PET and MRI. The PET/MR can observe combination with each advantage.

MATERIALS AND METHODS

1. General Remarks

Oleic acid-coated IO NP in chloroform was purchased from MKnano (MK Implex Corp., ON, Canada). The hydrodynamic diameter and size distribution of nanoparticles were analyzed using the DLS system from Zetasizer Nano ZS90 (Malvern Instruments Ltd., Worcestershire, U.K.) and transmission electron microscope (TEM) imaging using the JEM-1400 electron microscope (JEOL Ltd., Tokyo, Japan). A Scinco S-3100 was used for UV/Vis spectrometer (SCINCO America, WI, U.S.A.). The ^{68}Ge/^{68}Ga-generator was purchased from ITG (ITG GmbH, Munich, Germany). Instant thin layer chromatography-silica gel (ITLC-SG) was purchased from Agilent Technologies, Inc. (CA, U.S.A.). Radio-TLC was counted using a Bio-Scan AR-2000 System imaging scanner (Bioscan, WI, U.S.A.). Animal PET/CT imaging was performed using the eXplore Vista PET/CT scanner (GE Healthcare, CT, U.S.A.). Animal PET imaging was performed using the G4 PET X-RAY scanner (Sofie Biosciences, Culver City, CA, U.S.A.).The Agilent 9.4 T 160/AS MRI system and millipede coil (both radiofrequency transmission and signal reception) (Agilent Technologies, Santa Clara, CA, U.S.A.) were used for the MRI system.

All animal studies were performed at the Seoul National University Hospital, Seoul, Korea, which is fully accredited by AAALAC International (2007, Association for Assessment and Accreditation of Laboratory Animal Care International).

2. Synthesis

2.1. Synthesis of (S)-di-tert-butyl 2-(1H-imidazole-1-carboxamido) pentanedioate (2)

L-di-*tert*-butyl glutamate hydrochloride (1.50 g, 5.1 mmol) was dissolved in dichloromethane (DCM) (15 mL). The reaction mixture was cooled to 0^{o}C. Triethylamine (1.74 mL, 12.5 mmol) and 4-(dimethylamino)pyridine (DMAP) (3 pieces) were added to the reaction mixture. The reaction mixture was stirred for 5 min and 1,1`-carbonyldiimidazole (981 mg, 6.05 mmol) was added and warm to room temperature. The reaction mixture was stirred at room temperature for 18 h. The mixture was diluted with DCM (30 mL) and washed with saturated sodium bicarbonate (10 mL), water (2 × 10 mL), and brine (10 mL). The organic layer was dried over Na_2SO_4. The mixture was filtered and the filtrate was evaporated under reduced pressure. The crude material was solidified with hexane/ethyl acetate to afford a white solid which was filtered, washed with hexane (50 mL)..

2.2. Synthesis of (S)-1-((1,5-di-tert-butoxy-1,5-dioxopentan-2-yl)carbamoyl)-3-methyl-1H-imidazol-3-ium-4-ide (4)

(S)-di-tert-butyl 2-(1H-imidazole-1-carboxamido)pentanedioate (780 mg, 2.208 mmol) was dissolved in dichloroethane (DCE) (7.8 mL) and cooled to

0°C. Triethylamine (0.615 mL, 4.417 mmol), methyl trifluoromethanesulfonate (MeOTf) (0.252 mL, 2.230 mmol) were added to the reaction mixture and warm to room temperature. The reaction mixture was stirred at room temperature for 30 min. (S)-tert-butyl 2-amino-6-(((benzyloxy)carbonyl)amino)hexanoate (743 mg, 2.208 mmol) was added to the reaction mixture. The mixture was heat to 40°C and stirred for overnight. After finish this reaction, solvent was evaporated under reduced pressure. The compound was solidified with ether and n-hexane. Finally the compound **3** was obtained as white solid.

2.3. Synthesis of (9S,13S)-tri-tert-butyl 3,11-dioxo-1-phenyl-2-oxa-4,10,12-triazapentadecane-9,13,15-tricarboxylate

Ammonium formate (314 mg, 4.986 mmol) and 10 wt.% palladium carbon (100 mg) were added to a (S)-1-((1,5-di-tert-butoxy-1,5-dioxopentan-2-yl)carbamoyl)-3-methyl-1H-imidazol-3-ium-4-ide (310 mg, 0.499 mmol) in ethanol (5 mL). The reaction mixture was stirred at room temperature for 4 h. After the reaction was completed, the reaction mixture was filtered through Celite® 545 and washed with ethyl acetate (25 mL × 3). The filtrate was evaporated under reduced pressure. Finally the compound **4** as white solid.

2.4. Synthesis of (S)-di-tert-butyl 2-(3-((S)-6-amino-1-(tert-butoxy)-1-oxohexan-2-yl)ureido)

pentanedioate

(9S,13S)-tri-tert-butyl 3,11-dioxo-1-phenyl-2-oxa-4,10,12-triazapentadecane-9,13,15-tricarboxylate (47.8 mg, 0.0982 mmol), SCN-Bz-NOTA (55 mg, 0.0982 mmol) and trimethylamine (0.068 mL, 0.491 mmol) were suspended in chloroform (1.0 mL). This solution was stirred at rt for overnight. After finish this reaction solvent was removed under reduced pressure. The product was confirmed with MS by LC/MS system. : Mass spectrum (ESI^+), *m/z* = 939 $[M+H]^+$ observed.

2.5. Synthesis of 2,2',2''-(2-(4-(3-((S)-6-(tert-butoxy)-5-(3-((S)-1,5-di-tert-butoxy-1,5-dioxopentan-2-yl)ureido)-6-oxohexyl) thioureido)benzyl)-1,4,7-triazonane-1,4,7-triyl)triacetic acid

The crude mixture of (S)-di-tert-butyl 2-(3-((S)-6-amino-1-(tert-butoxy)-1-oxohexan-2-yl)ureido)pentanedioate was dissolved in trifluoroaceticacid/DCM solution (v/v : 1/1, 2.0 mL) and stirred at rt for 4 h. After 4 h the solvent was removed under reduced pressure and the residue was purified by HPLC system used MeCN and DW eluents. Final purified product **7** (**GUL-SCN-NOTA**) was collected and finally obtained as white solid by freeze drying. This solid purity and MS were confirmed with LC/MS system.

2.6. Synthesis of (2S)-2-(3-((1S)-1-carboxy-5-(3-(4-((1,4,7-tris(carboxymethyl)-1,4,7-triazonan-2-yl)methyl)phenyl)thioureido) pentyl)ureido)pentanedioic acid

$GaCl_3$ 0.5 M in pentane (1.242 mL, 0.621 mmol) and GUL-SCN-NOTA(**7**) (47.8 mg, 0.0621 mmol) were suspended in 1.0 M NaOAc buffer (2.0 mL, pH 5.6). The reaction mixture was stirred at rt for 8 h. After finish reaction the mixture was filtered through 0.2 μm pore syringe filter. And the filtrate was purified by silica gel column chromatography (ethyl acetate : n-hexane = 1 : 1, v/v) to obtain compound **2** as white solid.

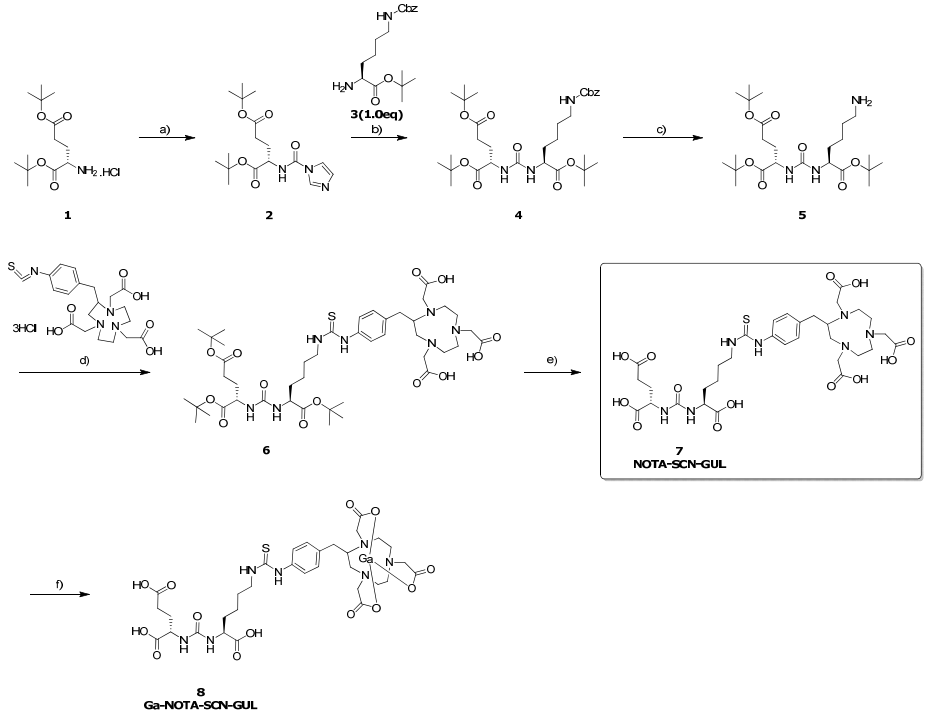

Scheme 1. Synthesis of NOTA-SCN-GUL

a) CDI, Et_3N, DMAP, DCM, 0°C to R.T., O/N, y:80% ; b) MeOTf, Et_3N, DCE, 0°C, 0.5hr ; (S)-tert-butyl 2-amino-6-(((benzyloxy)carbonyl)amino)hexanoate, 40°C, 1hr, y:86% ; c) Ammonium formate(10eq), 10%Pd-C, R.T, 2days, y:77% ; d) SCN-Bz-NOTA, Et_3N, DCM, R.T, O/N ; e) TFA/DCM, R.T, 4 h, y:63% ; f) $GaCl_3$, 1.0 M aqueous NaOAc solution, R.T, 8 h, y:58%

2.7. Synthesis of (S)-di-tert-butyl 2-(3-((S)-1-(tert-butoxy)-1-oxo-6-stearamidohexan-2-yl)ureido)pentanedioate

(S)-di-tert-butyl 2-(3-((S)-6-amino-1-(tert-butoxy)-1-oxohexan-2-yl)ureido) pentanedioate (300 mg, 0.616 mmol) was dissolved in dichloromethane (DCM) (1.0 mL). Stearoyl chloride (210 mL, 0.622 mmol) and triethylamine (129 mL, 0.923 mmol) were added to the solution. The reaction mixture was stirred at room temperature for 18 h. The organic layer was separated, washed with water (20 mL × 2), dried over Na_2SO_4. The mixture was filtered and the filtrate was evaporated under reduced pressure. The crude mixture was purified by silica gel column chromatography (ethyl acetate : n-hexane = 1 : 1, v/v) to obtain compound **2** as white solid. This solid purity and MS were confirmed with LC/MS system. Yield: 268 mg, 58%. Mass spectrum (ESI^+), *m/z* = 754.6 $[M+H]^+$ observed.

2.8. Synthesis of (S)-2-(3-((S)-1-carboxy-5-stearamidopentyl) ureido) pentanedioic acid (GUL-SA)

(S)-di-tert-butyl 2-(3-((S)-1-(tert-butoxy)-1-oxo-6-stearamidohexan-2-yl)ureido) pentanedioate (268 mg, 0.205 mmol) was dissolved in trifluoroacetic acid in DCM solution (9 mL, 2:1, v/v). The reaction mixture was stirred at room

temperature for 4 h. The reaction mixture was evaporated under reduced pressure. The crude mixture was purified by silica gel column chromatography (methanol : DCM = 1 : 9, v/v) to obtain compound **3** as white solid. Yield: 159 mg, 77%. ^{1}H-NMR ($CDCl_3$, 600 MHz) : δ (in ppm) =12.5 (bs, 3 H), 7.705 (t, J = 2.7 Hz, 1H), 6.294 (d, J = 4.2 Hz, 2 H), 4.062 (dd, J = 13.2, 7.8 Hz, 1H), 4.008 (dd, J = 13.2, 8.4 Hz, 1H) 2.972 (dd, J = 12.0, 5.4 Hz, 2H), 2.215 (dd, J = 15.0, 6.6 Hz, 2H), 2.001 (t, J = 7.2 Hz, 2H), 1.863 ~ 1.907 (m, 1H), 1.613 ~ 1.736 (m, 2H), 1.444 ~ 1.503 (m, 3H), 1.339 ~ 1.388 (m, 2H), 1.232 ~ 1.268 (m, 30H), 0.840 (t, J = 6.6 Hz, 3H). Mass spectrum (ESI^+), *m/z* = 586.7 $[M+H]^+$ observed.

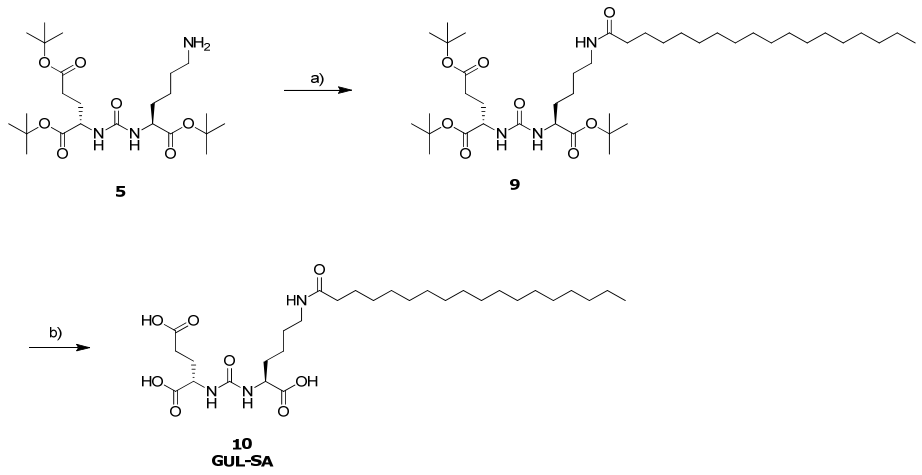

Scheme 2. Synthesis of GUL-SA

a) Stearoyl chloride, DIPEA, DCM, RT, O/N ; b) TFA, DCM, RT, O/N

2.9. Synthesis of 2,2',2'',2'''-(2-(4-(3-octadecylthioureido) benzyl)-1,4,7,10-tetraazacyclo dodecane-1,4,7,10-tetrayl) tetraacetic acid (DOTA-SA)

2,2',2",2"'-(2-(4-isothiocyanatobenzyl)-1,4,7,10-tetraazacyclododecane-1,4,7,10-tetrayl)tetraacetic acid (p-SCN-Bn-DOTA) (150 mg, 0.218 mmol) and stearyl amine (117.6 mg, 0.436 mmol) were dissolved in chloroform (2 mL). Triethylamine (91 μL, 0.654 mmol) was added to the mixture. The reaction mixture was stirred at room temperature for 8 h. The reaction mixture was evaporated under reduced pressure. The crude mixture was purified by silica gel column chromatography (methanol : DCM = 1 : 9, v/v) to obtain compound **5** (DOTA-SA) as white solid. Yield: 64 mg, 36%. ^{1}H-NMR (CD_3OD and $CDCl_3$ co-solvent, 600 MHz) : δ (in ppm) = 7.257 (dd, J = 27, 7.8 Hz, 2H), 7.143 (dd, J = 4.8, 7.8 Hz, 2H), 3.498 ~ 3.658 (m, 4H), 3.356 (t, J = 1.8, 1.2 Hz, 8H), 2.507 ~ 3.127 (m, 12H), 2.044 ~ 2.335 (m, 5H), 1.606 (bs, 2H), 1.264 ~ 1.324 (m, 30H), 0.872 (t, J = 7.2 Hz, 3H). Mass spectrum (ESI^+), *m/z* = 822.1 $[M+H]^+$ observed.

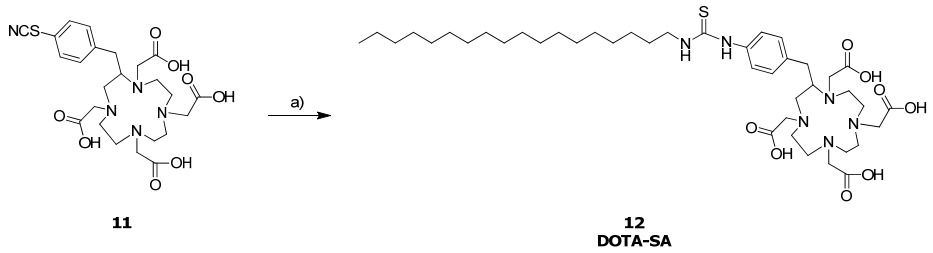

Shcme 3. Synthesis of DOTA-SA

a) Stearylamine, Et_3N, Chloroform, RT, O/N

3. Encapsulation of DOTA-IO-GUL

3.1. Preparation of the DOTA-IO-GUL nanoparticle

The DOTA-SA (2.57 mg, 3.19 μmol) and GUL-SA (3.27 mg, 3.19 μmol) were suspended in a solution of 8% Tween® 60 in distilled water (v/v, 1 mL) in a 2-mL glass vial. The reaction mixture was sonicated for 30 min using the ultrasonicator (77.8 W, Amplitude = 70%, cycle=1). Then, IO in chloroform (5 mg/mL, 100 μL) was slowly added. The reaction mixture was sonicated for 10 min and heated to 80°C for 10 min. This step was repeated 3 times for removing chloroform. After removing the chloroform, the reaction mixture was sonicated for 2 h (77.8 W, Amplitude=70%, cycle=1). Finally the reaction mixture was changed to clear dark brown color solution. The reaction mixture was purified by Sephacryl® S-500 HR-packed column chromatography (14.5 × 150 mm, V_0 = 2.37 mL) using distilled water as an eluent. The clean brown fractions were collected and concentrated by ultra-filtration (Amicon Ultra-0.5, 100 kDa, 5000 G, 30°C, 5 min).

3.2. Size analysis

DOTA-IO-GUL hydrodynamic diameter, size distribution and zeta potential were measured by the DLS instrument. Sample DOTA-IO-GUL (10 μL) was dissolved in distilled water (1 mL). This prepared sample was measured in a cuvette for DLS. The measured particle size and distribution were obtained in number-percent (%) value at 25^{o}C at a scattering angle of 90^{o}. Zeta potential was also measured by the DLS.

TEM was used for shape examination and size confirmation. Samples were diluted 100 times using distilled water and were dropped into the Ni coated metal grid. TEM images were obtained using an acceleration voltage of 80 keV.

3.3. Ferric ion concentration analysis

The Fe concentration of encapsulated DOTA-IO-GUL was analyzed using the iron thiocyanate colorimetric method. This method was based on Beer's law plot of iron(III) thiocyanate absorbance at 481 nm. Various concentrations of $Fe(NO_3)_3$ standard (0.1, 0.08, 0.06, 0.04, and 0.02 M), 0.5 M nitric acid and 1 M potassium thiocyanate solutions were prepared. Each 5 μL aliquot of $Fe(NO_3)_3$ and sample DOTA-IO-GUL solution was mixed with 1 mL of 0.5 M nitric acid solution. The mixture was incubated for 30 min at room temperature, and then 1 mL of 1 M potassium thiocyanate was added to each mixture. After

vortexing, the mixture was incubated for 30 min at room temperature. The absorbance of the resulting $Fe(SCN)^{2+}$ solution at 481 nm was measured by the UV-Vis spectrophotometer. The standard equation of standard Fe^{3+} concentration versus absorbance at 481 nm was drawn from the data by linear regression. The Fe^{3+} concentration of DOTA-IO-GUL was obtained from the equation and the absorbance of the sample.

3.4. Stability test in salt solution

The stability of DOTA-IO-GUL in a high salt solution was tested by the incubation of DOTA-IO-GUL in 0.9%, 1.8% and 3.6% NaCl (w/v) aqueous solution. These mixtures were incubated at room temperature and NP sizes were measured by DLS at 1 h, 12 h and 24 h.

4. Radiochemistry

4.1. ^{68}Ga labeling of DOTA-IO-GUL

$^{68}GaCl_3$ in 0.5 M hydrogen chloride (HCl) solution (200 μL, 111 MBq) was added to 1 M sodium acetate buffer (pH = 5.6, 200 μL). GUL-SCN-NOTA in aceteonitrile solution (10 μL, 1 mg/ 1 mL) was added and vigorously mixed for 1 min. The reaction mixture was incubated for 10 min at room temperature. Labeling efficiency of ^{68}Ga-GUL-SCN-NOTA was confirmed using ITLC-SG and 0.1 M Na_2CO_3 TLC eluent by radio TLC scanner.

4.2. Stability test in serum of ^{68}Ga-NOTA-SCN-GUL

^{68}Ga labeled GUL-SCN-NOTA stability was tested in human serum. ^{68}Ga-GUL-SCN-NOTA (3.7 MBq, 100 μL) was added to a vial in human serum (1 mL). This mixture was mixed with vigorous swing and vibration for 1 min and gently shaken at 36.5^{o}C in shaking incubator. After 2 h, the reaction mixture was tested by radio TLC system for radiochemical purity

4.3. ^{68}Ga labeling of DOTA-IO-GUL

$^{68}GaCl_3$ (111 MBq) in 0.1 M HCl solution (200 μL) was added to 1 M sodium acetate buffer (pH = 5.6, 200 μL). DOTA-IO-GUL (20 μL) was added

and vortexed for 1 min. The reaction mixture was incubated for 30 min at 90°C and was then cooled to room temperature. The labeling efficiency of ^{68}Ga-DOTA-IO-GUL was measured by ITLC-SG eluted with 0.1 M citric acid and scanned by the radio-TLC scanner. The medium of ^{68}Ga-DOTA-IO-GUL solution was replaced with distilled water by centrifugal ultrafiltration (0.4 mL, 3 times) and concentrated to 100 μL using the Amicon tube by centrifugation.

.

4.4. Stability test in human serum of ^{68}Ga-DOTA-IO-GUL

^{68}Ga-DOTA-IO-GUL (3.7 MBq, 100 μL) was added to human serum (1 mL) and was then vortexed vigorously. The mixture was incubated in a shaking incubator at 37.5°C. After 2 h, the radiochemical purity of the reaction mixture was tested by radio-TLC as described above. And also we compared the elution profiles of ^{68}Ga-DOTA-IO-GUL control and 2h after incubated ^{68}Ga-DOTA-IO-GUL in human serum determined by the Sephacryl® S-500 HR gel filtration chromatography (column : 14.5 × 150 mm).

5. *In vitro Assay*

5.1. Human prostate cancer cell culture

A PSMA-positive prostate cancer cell lines, 22Rv1(*56, 57*), and one PSMA-negative prostate cell line, PC-3, were used for this study. All prostate cancer cell lines were grown in a humidified incubator with a 5% carbon dioxide supply at 37°C. The 22Rv1 cell line was purchased from ATCC and was grown in ATCC-formulated RPMI 1640 (WELGENE Inc., Korea) mixed with 10% (v/v) heat inactivated fetal bovine serum (FBS) (Gibco®, Life Technologies Korea, Korea) containing 1% (v/v) antibiotic-antimycotic (100x) (Gibco®, Life Technologies Korea, Korea). The PC-3 cell lines was purchased from the Korean Cell Line Bank (KCLB, Seoul, Korea). The PC-3 cells were cultured in the same medium used for the 22Rv1 cell line.

5.2. in vitro competitive cell binding assay of Ga-NOTA-SCN-GUL

Competition binding analysis was used 22Rv1 for PSMA positive cell line. The 22Rv1 cells were plated in 24-well plates at approximately 2×10^5 cells/well and incubated for 24 h in a humidified incubator at 37°C, 5% CO_2. Ga-GUL-SCN-NOTA was diluted in serum–free cell culture medium containing 0.5% bovine serum albumin. Serial diluted Ga- GUL-SCN-NOTA samples were added to the cells in the presence of 1.85 kBq / 0.5 mL of ^{125}I

labeled (S)-2-(3-((S)-1-carboxy-5-((4-iodobenzyl)amino)pentyl) ureido)pentanedioic acid (^{125}I-MIP-1072) and incubated for 1 h in a humidified incubator at 37°C, 5% CO_2. After 1 h, the medium was aspirated and the pellet was washed twice by dispersal in fresh assay medium cells. The cells were removed from the plates by gently pipetting and transferred to 5 mL plastic test tubes. Radioactivity was counted with a γ-scintillation counter.

5.3. in vitro competitive cell binding assay of DOTA-IO-GUL

22Rv1 was used for competition binding analysis as PSMA-positive. The cells were plated in 24-well plates at approximately 2×10^5 cells/well and incubated for 24 h in a humidified incubator at 37°C with 5% CO_2 supply. DOTA-IO-GUL was serially diluted in a serum-free cell culture medium containing 0.5% bovine serum albumin. Each 0.5 mL of the diluted DOTA-IO-GUL sample was added to the cells with 1.85 kBq/0.5 mL of ^{125}I labeled (S)-2-(3-((S)-1-carboxy-5-((4-iodobenzyl)amino)pentyl)ureido)pentanedioic acid (^{125}I-MIP-1072)(*58*) and incubated for 1 h in a humidified incubator at 37°C with 5% CO_2. After 1 h, the media were aspirated and the pellet was washed twice by dispersal in fresh assay medium cells. One mL of 1% sodium dodecyl sulfate in phosphate buffered saline was added to each well and gently mixed to dissolve cells. The dissolved cells were transferred to 5-mL plastic test tubes. Radioactivity was counted by a gamma scintillation counter.

6. *In vivo and ex vivo Assay*

6.1. *Establishing a xenograft model*

Specific pathogen-free 4-wk old male BALB/c nude mice were used for all animal studies. 5×10^6 cells each of the 22Rv1 and PC-3 cell lines in 0.1 mL of RPMI-1640 medium were subcutaneously injected into the left and right flanks of mice, respectively. The xenografted tumors were grown for 2-3 weeks and then the mice were used for in vivo imaging studies.

6.2. *PET imaging study of ^{68}Ga-NOTA-SCN-GUL in mouse xenograft model*

Animal PET imaging study was used a PET/CT (Vista scanner, GE Healthcare, USA). ^{68}Ga-GUL-SCN-NOTA diluted in normal saline (6.04 MBq, 100 μL) was injected to 22Rv1 xenograft mice tail vain. After 1 h, the imaging was obtained by static mode for 10 min under isoflurane anesthesia. This PET images were acquired by 3-dimensional Fourier re-binning using a 2-dimensional ordered-subsets expectation maximization reconstruction algorithm using a MMWKS-Vista software. For each PET scan, 3-dimensional regions of interest (ROI) were drawn over tumors on whole body axial images. Standardized uptake values (SUV) were obtained using from reconstructed data for each PET imaging system. And the ^{68}Ga-GUL-SCN-NOTA diluted in

normal saline (5.85 MBq, 100 μL) and specific PSMA targeting small molecule MIP-1072 (50 mg/kg) were co-injected to 22Rv1 xenograft mice tail vain

6.3. PET imaging study ^{68}Ga-DOTA-IO-GUL in mouse xenograft model

^{68}Ga-DOTA-IO-GUL in normal saline (10.2 MBq, 100 μL) was injected into the 22Rv1 xenograft mice via the tail vein. After 1 h, images of the mice were obtained by static mode for 10 min under isoflurane anesthesia. These PET images were acquired by 3-dimensional Fourier re-binning using a 2-dimensional ordered-subsets expectation maximization reconstruction algorithm using the MMWKS-Vista software. For each PET scan, 3-dimensional regions of interest (ROI) were drawn over tumors on whole-body axial images. Standardized uptake values (SUV) were obtained using reconstructed data for each PET imaging system.

6.4. MRI imaging study in mouse xenograft model

A phantom study was performed to prove the dose-dependent MR signal acquisition. T2-weighted images were obtained using a phantom prepared with PCR tubes containing serially diluted DOTA-IO-GUL (200, 100, 50.0, 25.0, 12.5, 6.25 and 3.13 μM of ferric ion) in agarose solution. For animal MR imaging, 22Rv1 and PC-3 xenografted mice were used. The control MR image

was obtained before the DOTA-IO-GUL injection in anesthesia by isoflurane/O_2 (2% isoflurane, 1.0 L/min oxygen). The T2-weighted image was measured in fast spin echo multiple slice (FSEMS) Pulse sequence. The retention time was 3000 ms and the effective echo time was 29.0 ms. Echo Train Length (ETL) was 4, and the average was also 4. The matrix was 192 × 192 and the orientation was coronal. The field of view was 18.0 × 35.0 mm^2. The slices were 15 and slice thickness was 1.00 mm. After completion of the control MR imaging study, DOTA-IO-GUL 200 μM in 0.1 mL normal saline was injected into the tail vein of the mice. After 1 h, the T2-weighted MR image was obtained through the same method as control mice imaging. These MRI results were analyzed using the Sante DICOM viewer program.

RESULT

A. Result of NOTA-SCN-GUL small molecule

1 Chemistry

1.1. Synthesis of (S)-di-tert-butyl 2-(1H-imidazole-1-carboxamido) pentanedioate (2)

The final compound **2** as white solid. This product purity and mass were confirmed with LC/MS system. Yield: 1.44 g, 80%. Mass spectrum (ESI^+), *m/z* = 354 $[M+H]^+$ observed.

1.2. Synthesis of (S)-1-((1,5-di-tert-butoxy-1,5-dioxopentan-2-yl)carbamoyl)-3-methyl-1H-imidazol-3-ium-4-ide (4)

The final compound **3** was obtained as white solid. This product purity and mass were confirmed with LC/MS system. Yield: 1.18 g, 86%. Mass spectrum (ESI^+), *m/z* = 622 $[M+H]^+$ observed.

1.3. Synthesis of (9S,13S)-tri-tert-butyl 3,11-dioxo-1-phenyl-2-oxa-4,10,12-triazapentadecane-9,13, 15-tricarboxylate (5)

The final compound **4** as white solid. This solid purity and MS were

confirmed with LC/MS system. Yield: 243 mg, 98%. ^{1}H-NMR (DMSO-d6$_3$, 600 MHz) δ 8.43 (s, 1H), 8.10-7.10 (br, 1H), 6.50 (m, 2H), 4.01 (m, 1H), 3.92 (m, 1H), 2.69 (m, 2H), 2.17 (m, 2H), 1.83 (m, 1H), 1.70-1.49 (m, 4H), 1.38 (m, 27H), 1.29 (m, 2H).: Mass spectrum (ESI$^+$), *m/z* = 488 $[M+H]^+$ observed.

1.4. Synthesis of (S)-di-tert-butyl 2-(3-((S)-6-amino-1-(tert-butoxy)-1-oxohexan-2-yl)ureido) pentanedioate (6)

The product was confirmed with MS by LC/MS system. : Mass spectrum (ESI$^+$), *m/z* = 939 $[M+H]^+$ observed.

1.5. Synthesis of 2,2',2''-(2-(4-(3-((S)-6-(tert-butoxy)-5-(3-((S)-1,5-di-tert-butoxy-1,5-dioxopentan-2-yl)ureido)-6-oxohexyl) thioureido)benzyl)-1,4,7-triazonane-1,4,7-triyl)triacetic acid (7)

Final purified product **7** (**GUL-SCN-NOTA**) was collected and finally obtained as white solid by freeze drying. This solid purity and MS were confirmed with LC/MS system. Yield: 47.8 mg, 63% (2 steps overall yield). ^{1}H-NMR (DMSO-d6$_3$, 600 MHz) δ 12.4 (br, 6H), 9.45 (s, 1H), 7.69 (s, 1H), 7.38 (d, *J* = 8.10 Hz, 2H), 7.18 (d, *J* = 8.16 Hz, 2H) , 6.76 ~ 6.41 (br, 2H), 6.30

(m, 2H), 4.12-2.61 (m, 22H), 2.19 (m, 2H), 1.86 (m, 1H), 1.74-1.51 (m, 4H), 1.29 (m, 2H).: Mass spectrum (ESI^+), *m/z* = 770 $[M+H]^+$ observed.

1.6. Synthesis of (2S)-2-(3-((1S)-1-carboxy-5-(3-(4-((1,4,7-tris(carboxymethyl)-1,4,7-triazonan-2-yl)methyl)phenyl)thioureido) pentyl)ureido)pentanedioic acid (8)

The pyrified solid purity and MS were confirmed with LC/MS system. Yield: 268 mg, 58%. ^{1}H-NMR (DMSO-$d6_3$, 600 MHz) δ 12.4 (br, 3H), 9.45 (s, 1H), 7.69 (s, 1H), 7.38 (d, *J* = 8.10 Hz, 2H), 7.18 (d, *J* = 8.16 Hz, 2H) , 6.76 ~ 6.41 (br, 2H), 6.30 (m, 2H), 4.12-2.61 (m, 22H), 2.19 (m, 2H), 1.89 (m, 1H), 1.74-1.51 (m, 4H), 1.29 (m, 2H). : Mass spectrum (ESI^+), *m/z* = 837 $[M+H]^+$ observed

2 Radiochemistry

The GUL-SCN-NOTA was tested in radiolabeling study used ^{68}Ga. I can confirmed the radiolabeling efficiency as over 99% (R_f = 1.0) from radio TLC scanning and only less than 1.0% free ^{68}Ga (R_f = 0.0) remained. And also ^{68}Ga -GUL-SCN-NOTA can obtained as radio chemical purity more than 99% (**Figure 2**).

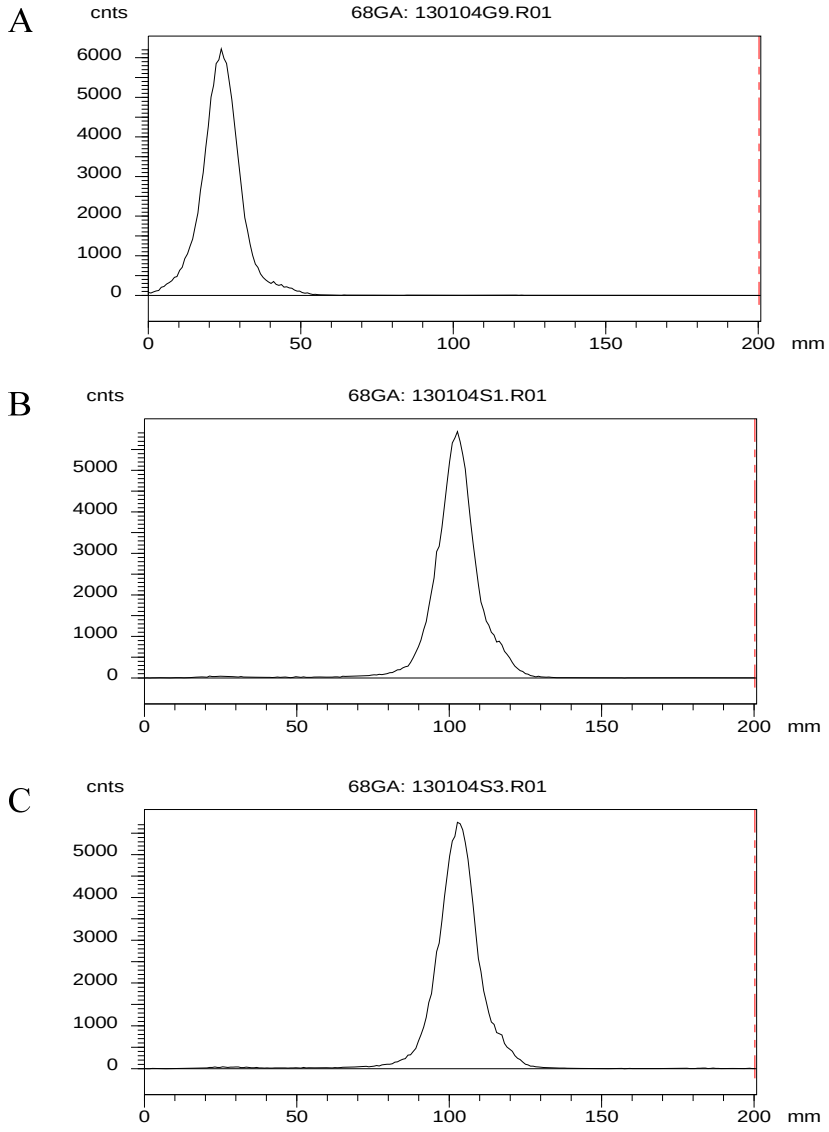

Figure 2. Radio TLC result in 0.1 M Na_2CO_3

A) Free $^{68}GaCl_3$; B) Labeling efficiency of ^{68}Ga-GUL-SCN-NOTA (>99%);

C) After 2 h incubated at 36.5^{o}C in human serum solution radio TLC result of ^{68}Ga-GUL-SCN-NOTA (>99%)

3 In vitro assay result

Competition binding analysis was used 22Rv1 for PSMA positive cell line (**Figure 3**). The 22Rv1 cells were plated in 24-well plates at approximately 2×10^5 cells/well and incubated for 24 h in a humidified incubator at 37°C, 5% CO_2. Ga-GUL-SCN-NOTA was diluted in serum–free cell culture medium containing 0.5% bovine serum albumin. Serial diluted Ga-GUL-SCN-NOTA samples each 0.5 mL were added to the cells in the presence of 1.85 kBq / 0.5 mL of ^{125}I labeled (S)-2-(3-((S)-1-carboxy-5-((4-iodobenzyl)amino)pentyl)ureido)pentanedioic acid (^{125}I-MIP-1072) and incubated for 1 h in a humidified incubator at 37°C, 5% CO_2. After 1 h, the medium was aspirated and the pellet was washed twice by dispersal in fresh assay medium cells. 1 mL of 0.5% sodium dodecyl sulfate in phosphate buffer saline solution was added to the plates and gently mixed for cell remove. The mixture was transferred to 5 mL disposable plastic test tubes. Radioactivity was counted by γ-counter

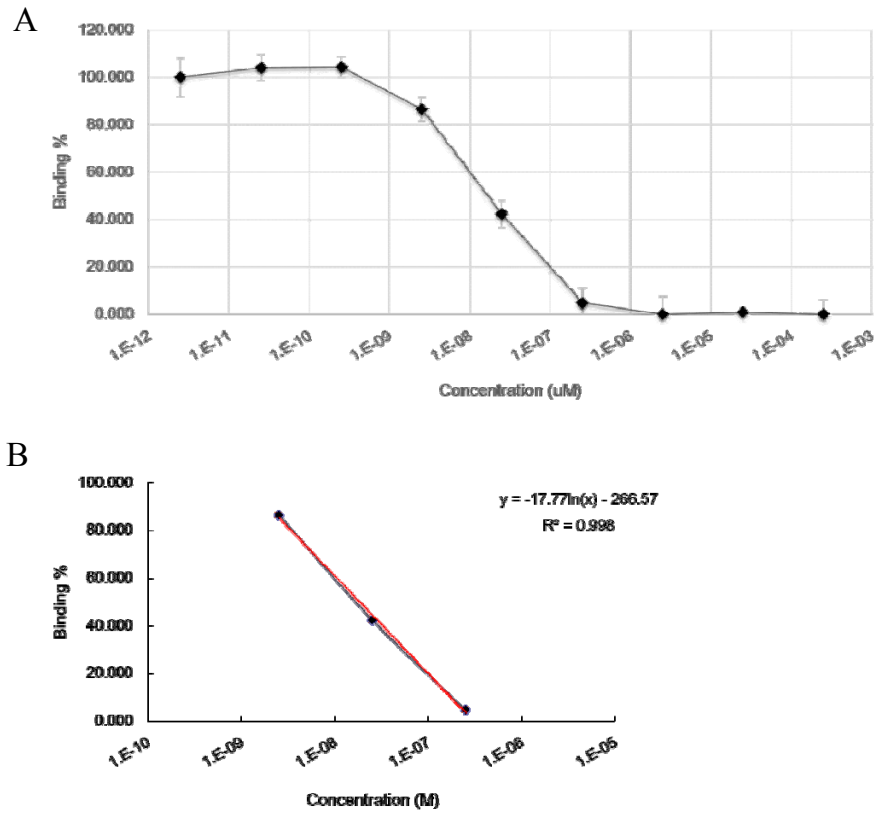

Figure 3 *in vitro* Cell binding assay result.

a) Measured radioactivity result curves in the 22Rv1 (PSMA positive cell line), Ga-GUL-SCN-NOTA competitively inhibited binding with ^{125}I-MIP-1072 (PSMA inhibitor); b) The value of Ga-GUL-SCN-NOTA IC_{50} was calculated through non-linear regression analysis (y = -17.77ln (x) – 266.57, R^2 = 0.998). The IC_{50} is 18.3 nM.

4 Animal study

4.1 In vivo xegnograft model study.

For PET imaging study, we used ^{68}Ga as radioisotope. The ^{68}Ga was prepared using ^{68}Ge/^{68}Ga generator. GUL-SCN-NOTA (20 μL, 26.0 nM) was used in ^{68}Ga labeling. After finish the labeling, ^{68}Ga-GUL-SCN-NOTA solution was dissolved in normal saline for mouse injection. The prepared ^{68}Ga-GUL-SCN-NOTA (6.04 MBq, 0.1 mL) was injected through tail vein. After 1h from injection, the PET image was obtained by PET/CT system. ^{68}Ga-GUL-SCN-NOTA did selectively uptake to prostate cancer (**Figure 4A**) and the SUVmean was 0.141. And more, we confirm the PSMA elective uptake concept through cold blocking image. Known PSMA selective small molecule MIP-1072 was co-injected through tail vein with ^{68}Ga-GUL-SCN-NOTA (5.85 MBq, 0.1 mL). This blocking study image shown ^{68}Ga- GUL-SCN-NOTA did not uptake to tumor (**Figure 4B**).

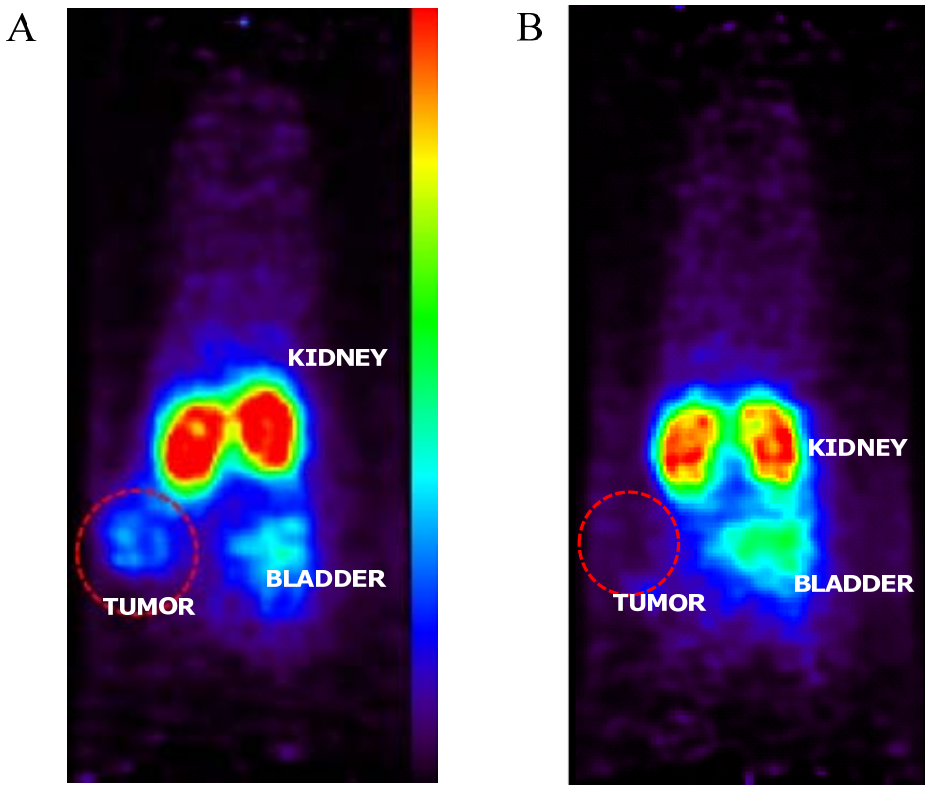

Figure 4. *in vivo* PET result.

a) PSMA selective uptake result in micro PET imaging. (SUV_{mean} : 0.141) ^{68}Ga-GUL-SCN-NOTA (2.85 MBq, 0.1 mL) tail vein injection after 1hr imaging. Tumor is PSMA positive tumor (22Rv1); b) Blocking study result with co-injection of MIP-1072 (50 mg/kg).

B. Result of DOTA-IO-GUL nanoparticle

1 Encapsulation of IO NPs

1.1 Formulation of IO NPs

The specific amphiphiles (S)-2-(3-((S)-1-carboxy-5-stearamidopentyl)ureido) pentanedioic acid (GUL-SA) and 2,2',2",2"'-(2-(4-(3-octadecylthioureido)benzyl)-1,4,7,10-tetraazacyclododecane-1,4,7,10-tetrayl)tetraacetic acid (DOTA-SA) were synthesized by 2- and 1-step reactions with 45% and 36% yields, respectively (**Scheme 2** and **3**). These amphiphiles were used for the encapsulation of IO core. The encapsulated NP DOTA-IO-GUL, a dark brown liquid, was obtained using the schematic method with a final yield is 85%. The prepared DOTA-IO-GUL has an IO core and a functionalized capsule composed of TWEEN 60, DOTA-SA and GUL-SA. TWEEN 60 provides a polyethylene glycol (PEG) side chain which allows it to escape from the immune system, known as the "stealth effect". The DOTA moiety is used for radiolabeling with metallic a radioisotope (^{68}Ga in this study) and the GUL moiety is used for targeting PSMA. The diameter of DOTA-IO-GUL, measured by dynamic light scattering (DLS), was 11.01 ± 1.541 nm (**Figure 6A**), which was confirmed by transmission electron microscopy (TEM) imaging (**Figure 6B**).

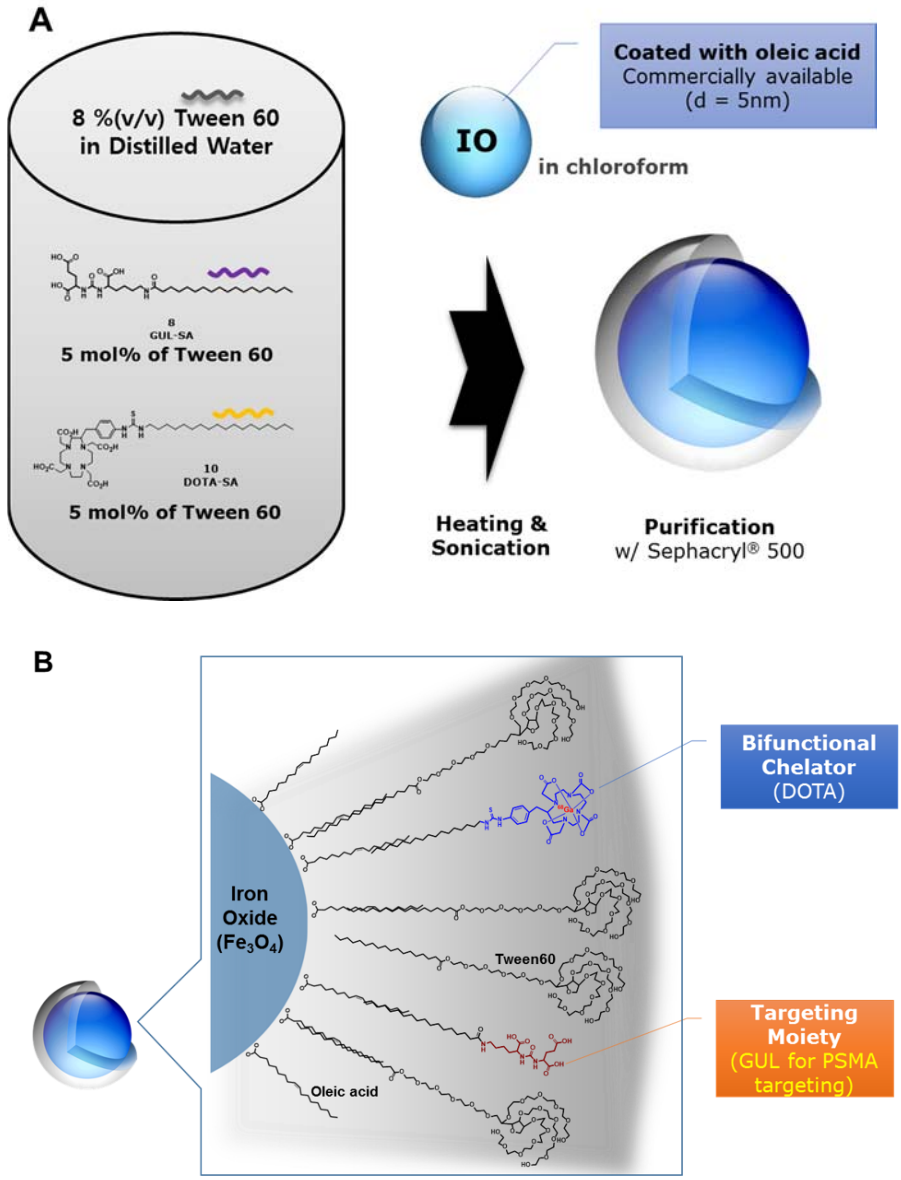

Figure 5. Diagram of Iron Oxide Nanoparticle.

(A) Encapsulation of NPs with specific amphiphiles. (B) Diagram of encapsulated DOTA-IO-GUL.

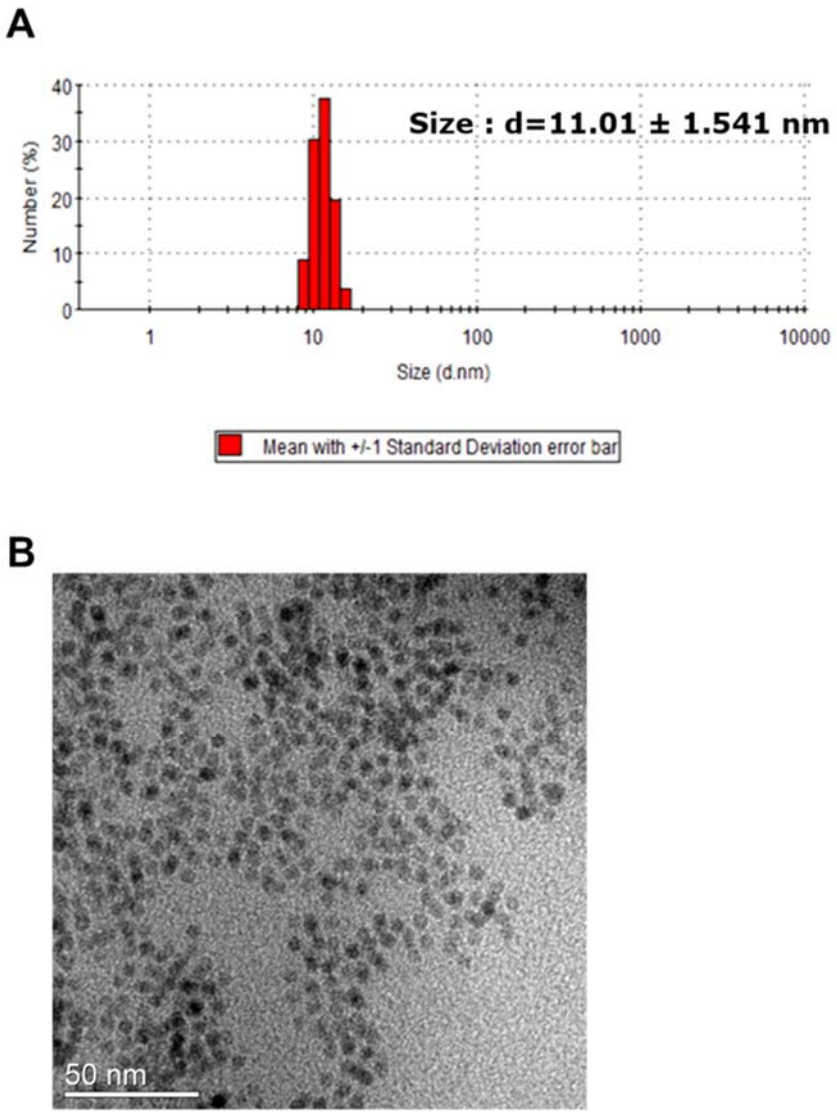

Figure 6. Size determination of DOTA-IO-GUL.

(A) DLS data of DOTA-IO-GUL (d = 11.01 ± 1.541 nm). (B) TEM image of DOTA-IO-GUL

1.2. Determination of ferric ion (Fe^{3+})

The iron oxide concentration was calculated follows below equation.

$$Fe^{3+}_{(aq)} + SCN_{(aq)} \rightleftharpoons [Fe(SCN)^{2+}]_{(aq)}$$

IO NPs were all decomposed to Fe^{3+} ion in HNO_3 aqueous solution and formed $[Fe(SCN)^{2+}]$ chelator after adding KSCN solution. After enough time for change the solution color to red, the wavelength of this solutions were detected by UV-Vis spectrometer (**Figure 7A**). And then, the absorbance data of five solutions at most high wavelength (at 481 nm) standard curve was calculated. The data was showed high correlation ($r^2 = 0.9993$) (**Figure 7B**). This standard equation was used to measure the concentration of Fe3+ from encapsulated DOTA-IO-GUL.

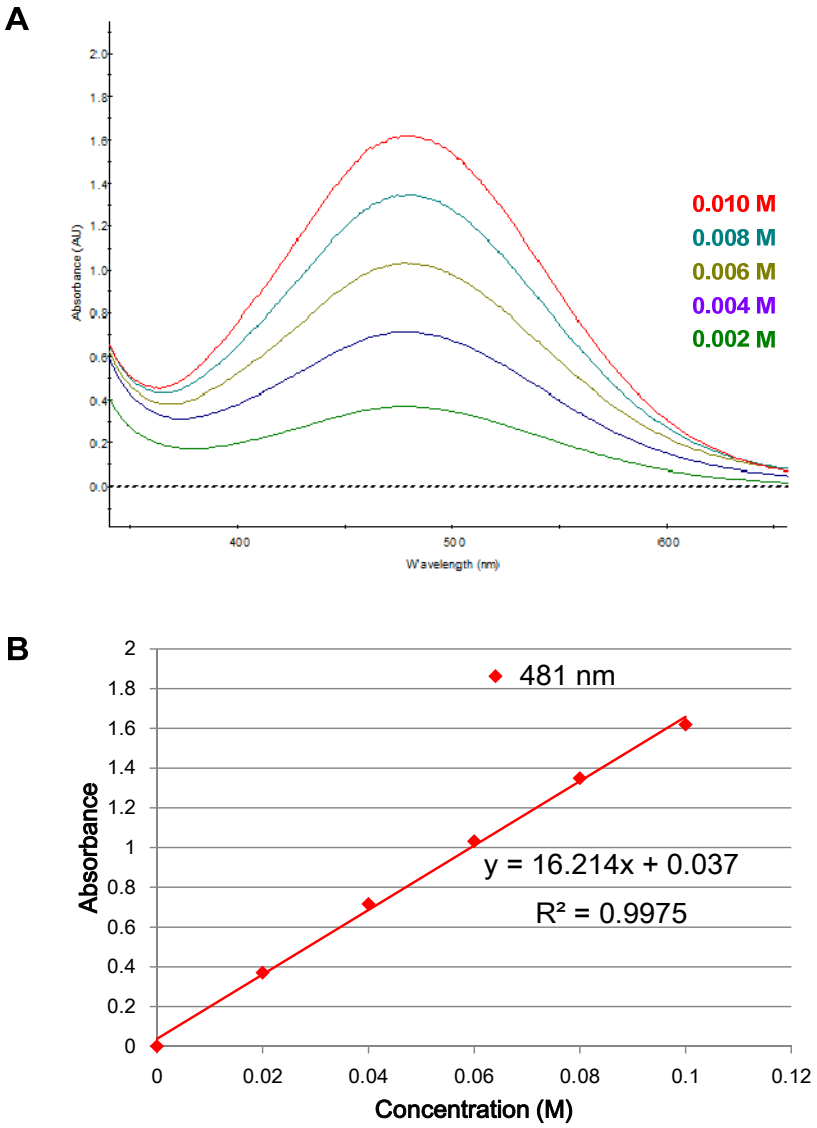

Figure 7. Colorimetric method of $[Fe(SCN)^{2+}]$.

(A) UV wavelength of $[Fe(SCN)^{2+}]$ in 5 different concentration ; (B) Standard equation of $[Fe(SCN)^{2+}]$ at 481 nm

2. Radiochemistry

The DOTA-IO-GUL was labeled with ^{68}Ga in a sodium acetate buffer (pH 5.6), with over 99% efficiency. According to radio thin layer chromatography (TLC) (ITLC-SG: solid phase, 0.1 M citric acid: mobile phase), ^{68}Ga-DOTA-IO-GUL remained at the origin (R_f = 0.0) and free ^{68}Ga moved with the solvent front line (R_f = 1.0). The medium of the radiolabeled mixture was replaced with distilled water by centrifugal ultrafiltration and then concentrated to 100 μL for the following experiments. The radiochemical purity of the final purified ^{68}Ga-DOTA-IO-GUL was higher than 99% (**Figure 8A**).

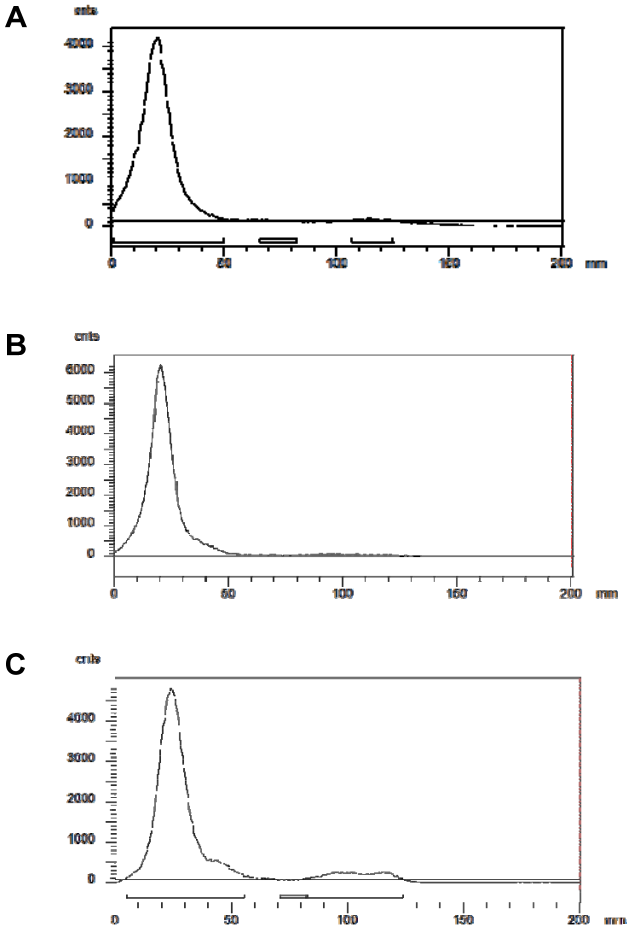

Figure 8. Radio TLC Result in 0.1 M Citric acid.

(A) Labeling efficiency of ^{68}Ga-DOTA-IO-GUL (99%); (B) Radiochemical purity (>99%); (C) After 2 h incubated at 36.5^{o}C in human serum solution radio TLC result of ^{68}Ga-DOTA-IO-GUL (94%)

3. Stability tests

NPs tend to aggregate in high salt solution which is one of the most common stability problems of NPs. In order to test the stability of DOTA-IO-GUL, it was incubated with various concentrations of NaCl aqueous solutions (0%, 0.9%, 1.8%, and 3.6%) for 24 h. Then the particle sizes of the solutions were measured using dynamic light scattering (DLS) to check for aggregation at 1, 12 and 24 h post-incubation (**Figure 9**). The results revealed that DOTA-IO-GUL size did not show any significant changes in the above conditions. This demonstrated that the prepared NP, DOTA-IO-GUL, is stable in salt solutions that are even 4-times more concentrated than physiological condition.

After being labeled with ^{68}Ga, the ^{68}Ga-DOTA-IO-GUL was incubated in human serum at 37^{o}C with shaking. The stability was checked by radio TLC after 2 h of incubation as mentioned in the Experimental section, and found to have 94% stability (**Figure 8C, Figure 10A**). Additionally I compared the elution profiles of ^{68}Ga-DOTA-IO-GUL and 2 h incubated ^{68}Ga-DOTA-IO-GUL on the Sephacryl® S-500 HR gel filtration chromatography (**Figure 10B)**. From this result I could not found a significant change of elution profile. It means the ^{68}Ga-DOTA-IO-GUL particle size also stable in human serum at 36.5^{o}C.

According to these in vitro experimental results, I found that ^{68}Ga-DOTA-IO-GUL is stable enough to be used as a PET probe.

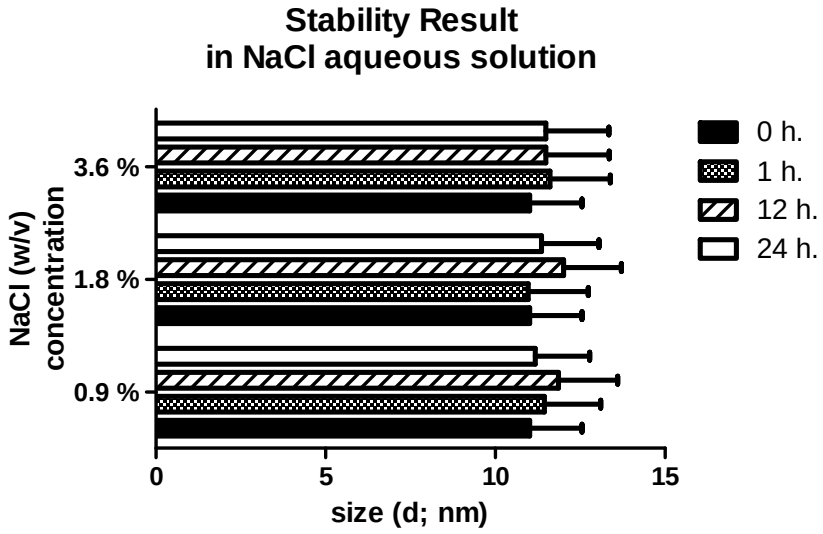

Figure 9. DOTA-IO-GUL stability study

in 0.9%, 1.8% and 3.6% NaCl solutions for 1 h, 12 h and 24 h.

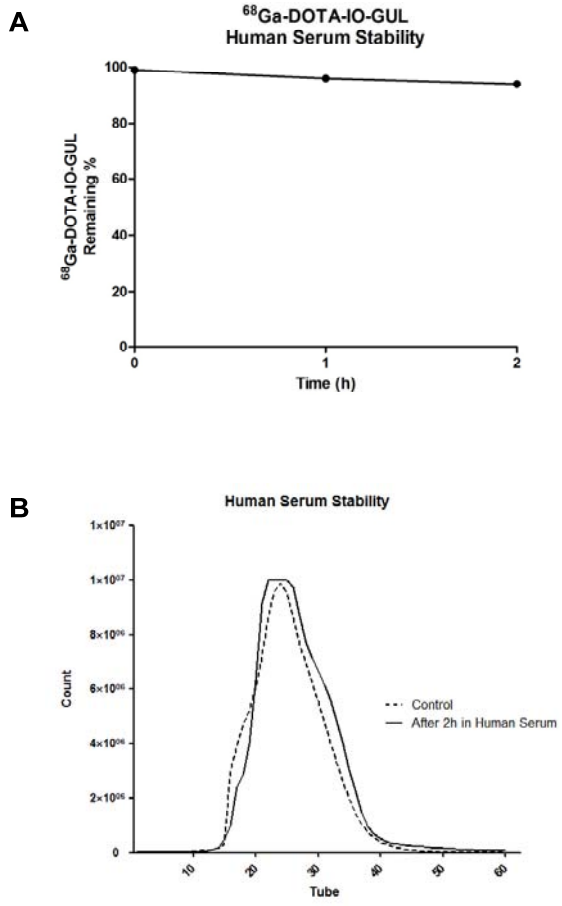

Figure 10. ^{68}Ga-DOTA-IO-GUL stability study in human serum for 2 h at 36.5ºC.

(A) Radiochemical purity (%) of ^{68}Ga-DOTA-IO-GUL in human serum. (B) Elution profiles of ^{68}Ga-DOTA-IO-GUL control and 2h after incubated ^{68}Ga-DOTA-IO-GUL in human serum determined by the Sephacryl® S-500 HR gel filtration chromatography.

4. Competitive binding study using a PSMA-positive cell line

Specific binding of DOTA-IO-GUL to PSMA-positive cells was confirmed by an in vitro competitive binding study. A previously reported PSMA-imaging agent, ^{123}I-MIP-1072, was used as a radiolabeled ligand.(*58, 59*). The PSMA-positive human prostate cancer cell line, 22Rv1, was incubated with ^{125}I-MIP-1072 and various concentration of DOTA-IO-GUL at room temperature for 1 h. After the aspiration of unbound fractions, the cell-bound radioactivities were measured. A binding curve with dose-dependent blocking was obtained (**Figure 11**), which proved the specific binding of DOTA-IO-GUL to PSMA-positive cells.

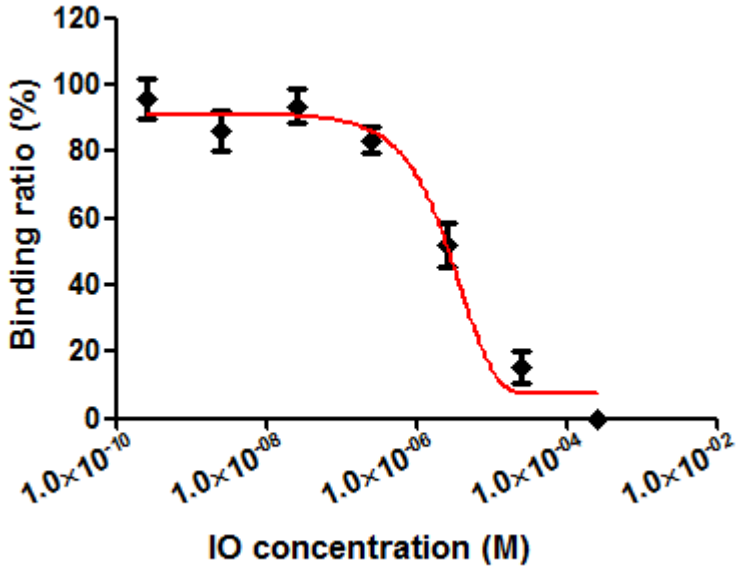

Figure 11. ***In vitro*** **cell binding assay result.**

Bound radioactivity of ^{125}I-MIP-1072, a PSMA-inhibitor, to the PSMA-positive cells, 22Rv1, showed a dose-dependent decrease by addition of DOTA-IO-GUL.

5. MRI phantom study

MR imaging of a phantom composed of serially diluted aqueous solutions of 200 μM DOTA-IO-GUL demonstrated the linearity of T2-weighted MR signal with IO concentrations (**Figure 12**).

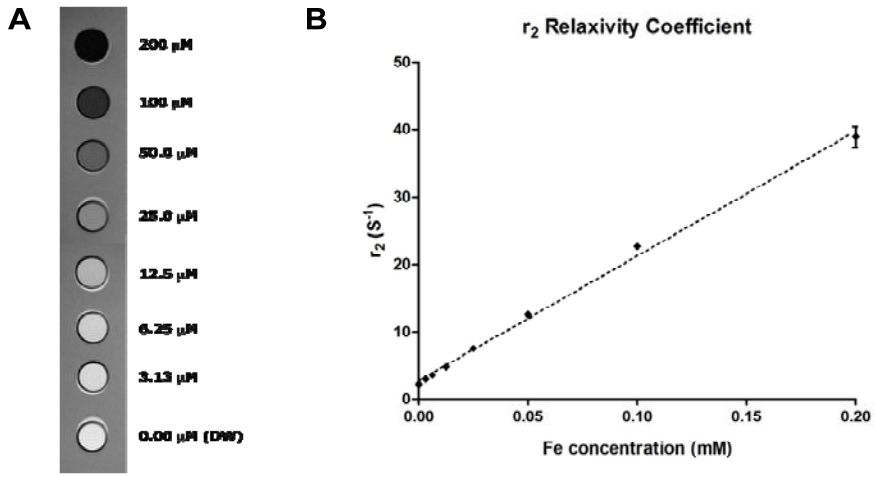

Figure 12. MRI phantom study for the determination of DOTA-IO-GUL injection concentration.

(A) MR image was obtained from serially diluted DOTA-IO-GUL from 200 μM Fe^{3+} concentration. (B) Calculation of r_2 relaxivity coefficient value of DOTA-IO-GUL ($y = 185.13 x + 2.6898$; $R^2 = 0.9968$).

6. In vivo Animal study

6.1. MRI imaging study using a single xenograft model

For in vivo imaging studies, a BALB/c mouse model having prostate cancer xenografts of the PSMA-positive cell line (22Rv1) at the left flank was established. The 22Rv1 tumor MR image taken before administration of NOTA-IO-GUL was shown to be bright gray masse (**Figure 13A**). However, decreased MR signals (as block dots) were found with the 22Rv1 tumor, representing increased uptake of IO NPs at an after 1h from injection of DOTA-IO-GUL. This result shown that DOTA-IO-GUL was taken up by the PSMA-positive 22Rv1 tumor (**Figure 13B**).

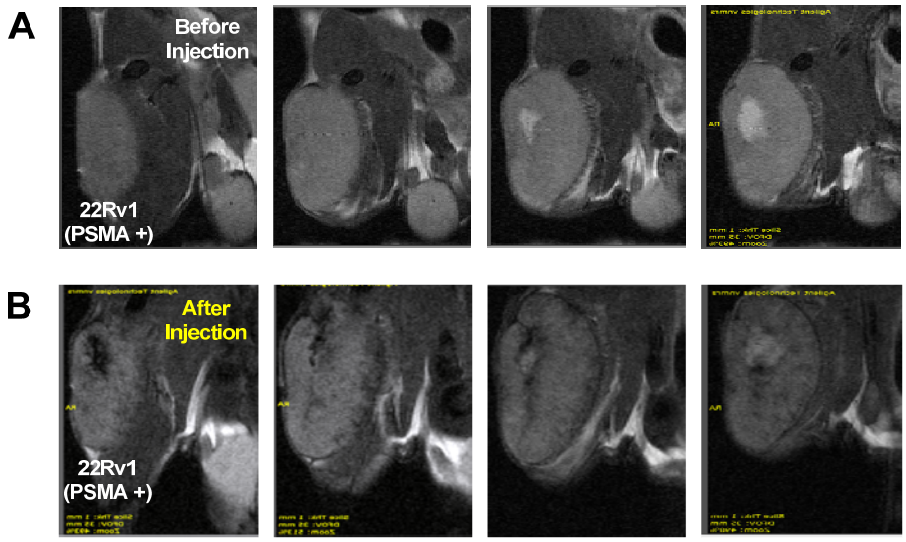

Figure 13. *In vivo* micro MRI image results.

(A) Before injection, control images; (B) After injection of DOTA-IO-GUL (0.1 mL, 0.2 mM) through the tail vein (1 h). The tumor is PSMA positive (22Rv1).

6.2. in vivo PET imaging study using a single xenograft model

PET images was obtained 1 h post-injection of ^{68}Ga-DOTA-IO-GUL through the tail vein. (**Figure 14**). And the PSMA-specific uptake could be proved by a blocking study in vivo using PET imaging. A known PSMA-specific small molecule, MIP-1072, was co-injected with ^{68}Ga-DOTA-IO-GUL through the tail vein, and it was found that ^{68}Ga-DOTA-IO-GUL uptake was blocked (**Figure 15**). The specific uptake of ^{68}Ga-DOTA-IO-GUL by the PSMA-positive tumor was proven by these results.

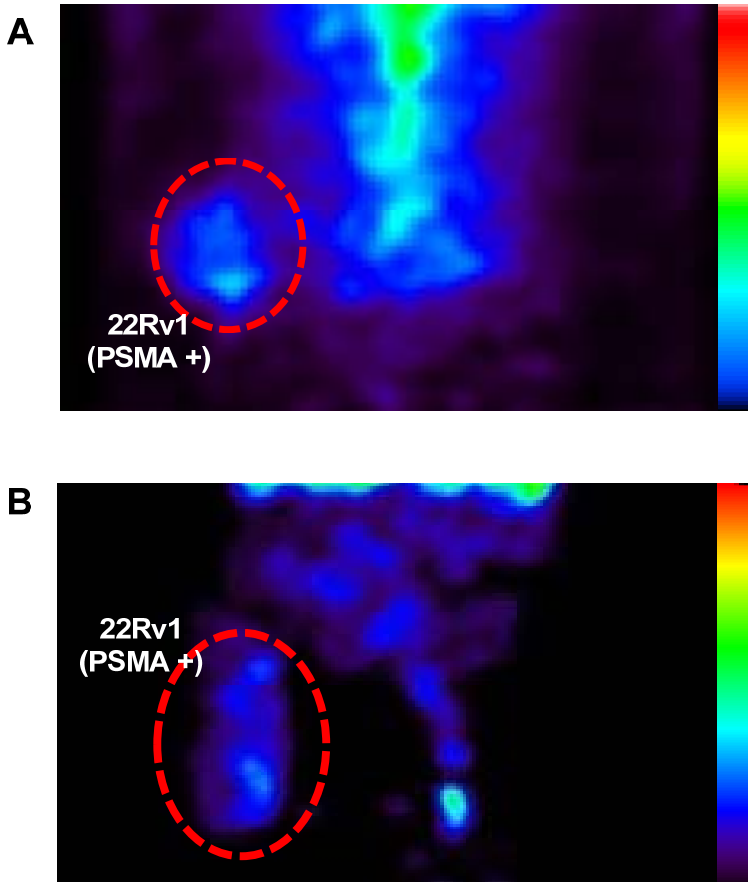

Figure 14. ***In vivo*** **PET result**. **PSMA-selective uptake results in micro PET imaging.**

(A) mouse 1 was injected ^{68}Ga-DOTA-IO-GUL (3.77 MBq, 0.1 mL) and (B) mouse 2 was injected ^{68}Ga-DOTA-IO-GUL (2.22 MBq, 0.1 mL) (Tail vein injection after 1 h imaging. The Tumor is PSMA-positive (22Rv1)).

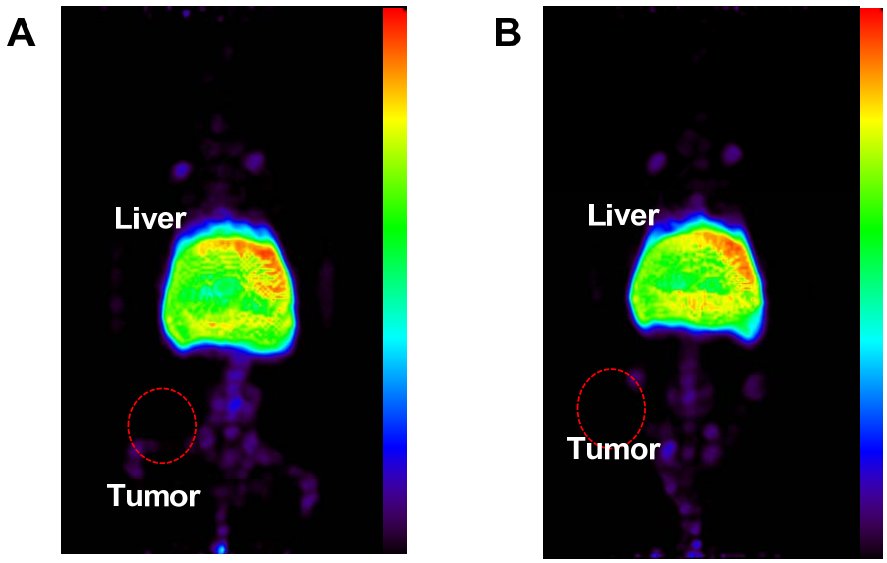

Figure 15. *In vivo* PET result. : Blocking study result with co-injection of MIP-1072 (50 mg/kg) in micro PET imaging.

(A) mouse 1 was injected ^{68}Ga-DOTA-IO-GUL (3.77 MBq, 0.1 mL) and (B) mouse 2 was injected ^{68}Ga-DOTA-IO-GUL (3.82 MBq, 0.1 mL) (tail vein injection after 1 h imaging. The Tumor is PSMA-positive (22Rv1)).

6.3. MRI imaging study using a dual xenograft model

For in vivo imaging studies And also I tried *in vivo* imaging studies, a BALB/c mouse model having prostate cancer xenografts of the PSMA-positive cell line (22Rv1) and PSMA-negative cell line (PC-3) at the left and right flank, respectively, was established. Both of the 22Rv1 and PC-3 tumor MR images taken before administration of NOTA-IO-GUL were shown to be white masses (**Figure 16A**). However, decreased MR signals were found with the 22Rv1 tumor, representing increased uptake of IO NPs after an injection of DOTA-IO-GUL, while the PC-3 tumor did not show any change. This result demonstrated that DOTA-IO-GUL was only taken up by the PSMA-positive 22Rv1 tumor and not by the PSMA-negative PC-3 tumor (**Figure 16B**). On the other hand, this MR imaging study could not provide quantitative information on tumor uptake.

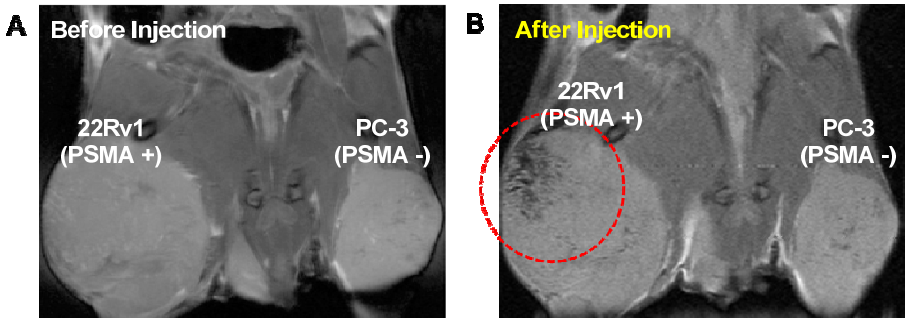

Figure 16. *In vivo* micro MRI image results.

(A) Before injection, control image; (B) After injection of DOTA-IO-GUL (0.1 mL, 0.2 mM) through the tail vein (1 h). Left tumor is PSMA positive (22Rv1) and right tumor is PSMA-negative (PC-3). Red circle demonstrates the selective uptake of DOTA-IO-GUL to the positive tumor (49.1 Fe ng/g).

6.4. PET imaging study using a dual xenograft model

For in vivo imaging studies All of PET images were obtained 1 h post-injection of ^{68}Ga-DOTA-IO-GUL through the tail vein, and the uptake of ^{68}Ga-DOTA-IO-GUL was found only in the 22Rv1 tumor, which was consistent with the MR imaging study (**Figure 17**). However, the resolution of PET images were much lower than MR images. The obviously dotted MR images showed localized distribution in the tumor with higher resolution than PET. On the other hand, the PSMA-specific uptake could be proved by a blocking study in vivo using PET imaging. A known PSMA-specific small molecule, MIP-1072, was co-injected with ^{68}Ga-DOTA-IO-GUL through the tail vein, and it was found that ^{68}Ga-DOTA-IO-GUL uptake was blocked (**Figure 18**). The specific uptake of ^{68}Ga-DOTA-IO-GUL by the PSMA-positive tumor was proven by these results.

In addition, the PET imaging study could be used for the quantification of tumor uptakes. The amount of the injected ^{68}Ga-DOTA-IO-GUL was 1.544 μg. The standard uptake value (SUV) of the 22Rv1 tumor was calculated as 2.385 from the PET image, and the amount of IO in the 22Rv1 tumor was calculated to be 0.0825 μg.

Based on these imaging studies, it was demonstrated that MR images shows a higher resolution of tumor uptake, and PET images can confirm the specific uptake and provide quantitative results of tumor uptake.

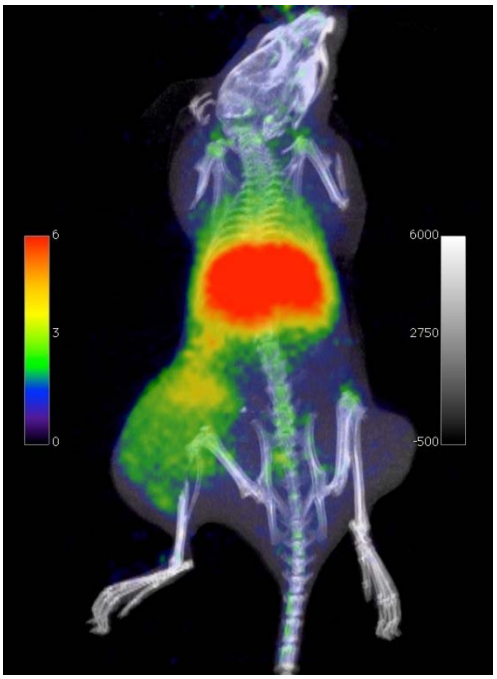

Figure 17. *In vivo* PET result – Selective tumor uptake.

PSMA-selective uptake result in micro PET imaging. (SUV_{mean} = 0.668) ^{68}Ga-DOTA-IO-GUL (10.2 MBq, 0.1 mL) tail vein injection after 1 h imaging. Left tumor is PSMA-positive (22Rv1) and right tumor is PSMA-negative (PC-3)

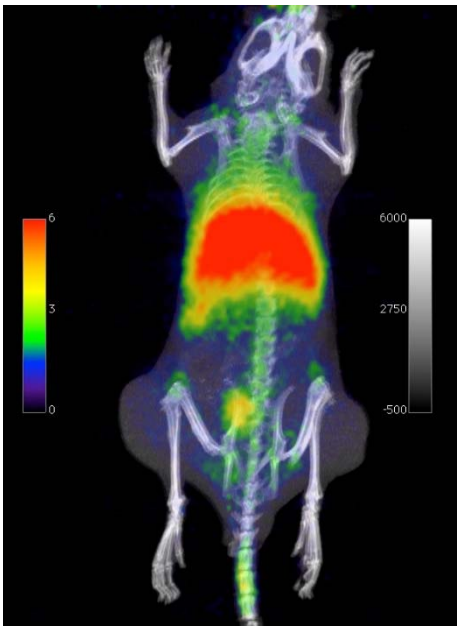

Figure 18. *In vivo* PET result – Blocking study.

Tumor blocking study result in micro PET imaging. ^{68}Ga-DOTA-IO-GUL (10.2 MBq, 0.1 mL) and PSMA targeting small molecule MIP-1072 (50 mg/kg) were co injected through tail vein injection after 1 h imaging. Left tumor is PSMA-positive (22Rv1) and right tumor is PSMA-negative (PC-3).

Table 2. ***In vivo*** **IMAGING RESULT – PET and MRI**

MRI image 1 h after from injection	control	PET image 1 h after from injection
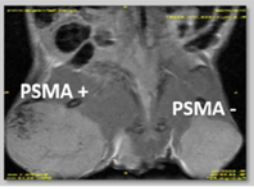		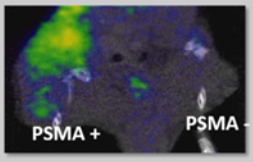
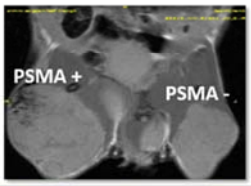	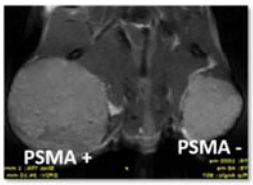	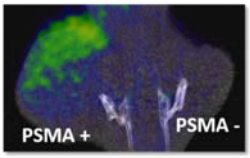
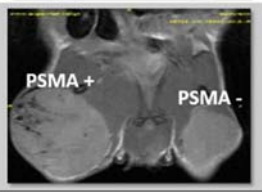		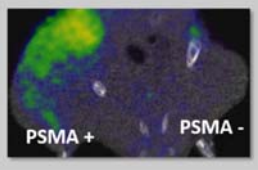

All of images are section coronal image. All of MRI (Left) and PET (Right) result shown a selectively uptake in PSMA positive tumor.

Table 3. COMPARISON of NANOPARTICLE (DOTA-IO-GUL) and SMALL MOLECULE (NOTA-SCN-GUL).

	DOTA-IO-GUL	NOTA-SCN-GUL
Morphology	Nanoparticle	Small molecule
PET imaging result	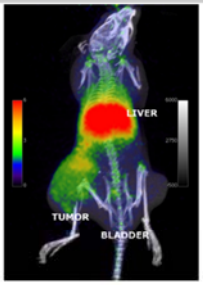	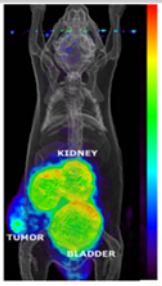
MRI imaging	possible	impossible
Most highest uptake organ	Liver	Bladder (2nd: Kidney)
Advantage	• Low uptake in bladder • Multimodality	• Correct Concentration measurement possible
Disadvantage	• Correct Concentration measurement difficulty	• High bladder uptake

The characteristics compared with DOTA-IO-GUL(nanoparticle) and NOTA-SCN-GUL(small molecule).

DISCUSSION

Nanomedicine is an attractive research topic to a medicinal chemist. During last few years, many groups challenge to the development of new nanoparticles for medicinal application. Nevertheless, the modification method of nanoparticle has limitation about encapsulation of nanoparticle. Our research group was already developed and published new method which is improved nanoparticle modification method with high reproducibility and scalability. In this study, I developed a novel nanoparticle as multimodality imaging probe by the newly developed one-pot method with iron oxide, DOTA and PSMA targeting moiety.

Iron oxide has a good advantage for using in clinical application to avoid toxicity because the basis of IO is iron which exists in abundantly in the human body particularly in blood. And also IO-based nanoparticles are one of the best options for an MRI imaging contrast. Thus, IO NPs are known to be less toxic than a gadolinium (Gd)-based MR contrast agents (*60*). In the present study, DOTA-IO-GUL was prepared by the encapsulation of oleic acid-coated IO NPs using special amphiphiles such as GUL-SA, NOTA-SA and TWEEN 60. GUL-SA and NOTA-SA were easily prepared by organic synthesis.

The DOTA-IO-GUL has bifunctional chelator DOTA for radioisotope labeling. After radioisotope labeling, this nanoparticle can be used in nuclear medicinal imaging such as PET. In here DOTA-IO-GUL was labeled with ^{68}Ga for PET imaging.

DOTA-IO-GUL can be used in MRI due to iron oxide core and also used in PET imaging system by ^{68}Ga labeling in DOTA. In addition, the DOTA-IO-GUL can be used in PET/MR imaging also possible due to DOTA-IO-GUL is combined with iron oxide and DOTA. The PET/MR is an attractive imaging tool for the next generation of the molecular imaging field. MR imaging can provide high-resolution anatomical imaging, while PET imaging can provide specific binding and quantitative information. In addition, PET can provide images with high sensitivity to microdoses of radioisotopes. Development of an efficient and reliable PET/MR dual-imaging probe is essential to actualize the PET/MR instrument`s powerful application. DOTA-IO-GUL can be used in not only PET, MRI and also PET/MR.

DOTA-IO GUL has also GUL moiety for PSMA specific uptake. The PSMA is highly strong targeting moiety for prostate cancer and the metastasis. Prostate cancer is now one of the most rapidly increasing types of men cancer in world-wide. The GUL structure is a specific PSMA-targeting moiety. In here, I can develop PSMA targeting imaging probe for PET, MRI, and PET/MR multimodality imaging probe for early and accurate diagnosis of prostate cancer is extremely.

The prepared NP, ^{68}Ga-DOTA-IO-GUL, showed high radiolabeling efficiency at pH 5.6 and was stable in high-salt concentration. The specific binding of ^{68}Ga-DOTA-IO-GUL to PSMA-positive cells was confirmed *in vitro* and *in vivo*. PET and MR images were obtained by using an adequate amount of radioactivity and cold NPs to adjust the sensitivity of each modality. MR

images showed a high uptake of the NP by the PSMA-positive tumor with high resolution, but was limited in providing quantitative information. PET images also showed specific uptake by the PSMA-positive tumor, and furthermore provided quantitative information. With this information, the amount of IO NP accumulated in the tumor could be calculated. However, the resolution of PET images were lower than the MR images. In this study, the image data were obtained from each of PET and MRI respectively, nevertheless the each results were shown the ^{68}Ga-DOTA-IO-GUL can be used for PET/MR dual-imaging probe of prostate cancer likewise (**Table 2**).

The uptake of NPs by tumor is often associated with the enhanced permeability and retention (EPR) effect, which can occur with nanoparticles to any kind of tumors, non-specifically (*61-63*). On the other hand, in this study, I used a PSMA-positive and PSMA-negative tumor xenografted mouse model to prove the specificity. Uptake of DOTA-IO-GUL was revealed only in the PSMA-positive tumor by both PET and MR imaging. If the DOTA-IO-GUL uptake by the tumor was by the EPR effect, the uptake might be exhibited in both the PSMA-positive and negative tumors. I also proved by PET imaging that the uptake of DOTA-IO-GUL could be blocked by a PSMA-binding agent, which definitely demonstrated that the uptake was followed specific binding mechanism but not EPR effect.

In this experiment, I could distinguish the specific uptake of DOTA-IO-GUL to the PSMA-positive tumor by MR imaging in a mouse model xenografted with both PSMA-positive and negative tumors. And MR images were obtained

both before and after administration of DOTA-IO-GUL. However, in clinical settings, MR imaging would produce gray tumor images which would make it almost impossible to distinguish whether it is positive or not. Thus, the cancer specificity can be provided only by PET imaging, but not by MR imaging in clinical practice.

Another important point to consider about the PET/MR dual-imaging agent is the different sensitivities of PET and MRI. One of the most important advantages of PET is its high sensitivity, thus microdosing of the contrast agent is enough to obtain high quality imaging (*64*). Although PET can provide us with highly specific images, it tends to produce images with low resolution. Positron emitters can travel a few millimeters before annihilation occurs, which is a cause of decreasing resolution. In addition, the partial volume effect also affects resolution, especially in small objects. These are intrinsic problems of PET imaging, which can be compensated by a simultaneous MRI or CT. On the other hand, due to its low sensitivity, a much higher dose of contrast agent is required for MR imaging than PET. In order to solve this problem, microdose of ^{68}Ga-DOTA-IO-GUL having a high enough radioactivity (10.2 MBq) was used for PET imaging and cold DOTA-IO-GUL having enough concentration for MRI contrast agent (0.2 M) was used for MR imaging in this study. Thus, I could obtain both PET and MR images.

In this study, I also confirmed the characters of DOTA-IO-GUL from comparison with PSMA targeted small molecule, NOTA-SCN-GUL (**Table 3**). Both of nanoparticle and small molecule were shown a high uptake at a tumor.

However, the small molecule PET imaging was shown a high uptake in bladder and kidney. The prostate is close to the bladder. So high uptake of radioactivity in bladder region is one of the most serious problem to detection of prostate cancer. Unfortunately, many of small molecule has can be excreted by the kidney and renal. In contrast, the nanoparticle has no problem about high bladder uptake. From the ^{68}Ga-DOTA-IO-GUL PET image, the nanoparticle was not shown a high uptake to kidney and renal region. It is one of the strong point of why PSMA targeted nanoparticle is good to use in prostate cancer than a small molecule.

Although PSMA targeted nanoparticle has the advantage to using in prostate cancer, the limitation also existed. I studied measurement of nanoparticle mass with MALDI/TOF and calculation method. However, it was difficult to obtain a reliable data due to PEG structure. Nevertheless, this limitation is not serious to the radiopharmaceutical. A small molecule, especially using for pharmaceuticals have to inject the active dose such as more than IC_{50} or EC_{50}. The activity and active dose have important meaning to medicines. On the other hand in radiopharmaceutical part, the important meaning and concept are focused on the injected radio activity. The radiopharmaceutical was used the only trace amount of chemical, such as nanograms (10^{-9} g) scale. This concentration is not enough any biological toxicity in the human body. And also this concentration is not enough to biological action when DOTA-IO-GUL was bind to the PSMA. It is enough to send a signal although trace amount bound to target. In contrast, when DOTA-IO-GUL used in MRI, the injection dose is determined by iron concentration. The iron concentration of DOTA-IO-

GUL can be measured by UV spectra. In this study, I already showed the measurement method and result (**Figure 7**).

Finally, I could confirm reproducibility and scalability of the original one-pot method developed from our study group. From this result, I could develop the PSMA targeting iron oxide nanoparticle. The nanoparticle was performed by 8% Tween 60 in DW solution based and mixed with GUL-SA and DOTA-SA as 5 mol% of Tween. This condition was optimized from previous work and reported (*21, 22, 65*). In this conditions the targeting moiety or bifunctional chelator can be changed according to the target disease or different radioisotope. However, the optimized concentration should not change for reproducibility.

Additionally, DOTA-IO-GUL can be labeled not only with ^{68}Ga but also with therapeutic beta emitters such as ^{90}Y or ^{177}Lu which have low penetration and high cytotoxic effects. Therefore, it has a possibility of being used for theragnostic application in the future although high uptake in the liver.

Despite these promising results, implementation issues still remained. At first, I should confirm the measurement of how many GUL moiety and NOTA is attached to this nanoparticle. Also, I should develop the quantification of nanoparticle method for wide application of the original one-pot method. And more the DOTA-IO-GUL are going to obtain the imaging result in PET/MR system. In this study, the imaging results are obtained PET and MRI respectively. However in the future study, the PET/MR data also obtain in PET/MR system. At last, the DOTA-IO-GUL should study for therapeutic effect using labeled with therapeutic radioisotope compound. If the DOTA-IO-

GUL theragnosis is possible, the DOTA-IO-GUL can be more powerful candidate for prostate cancer patient.

In summary, I can develop a PSMA-targeting IO NP by the original one-pot modification method developed by our lab. The IO NP was encapsulated with specially prepared amphiphiles. The PSMA-targeting IO NP, DOTA-IO-GUL, is good to use for PET and MRI respectively. In addition, the DOTA-IO-GUL can be used in PET/MR imaging also possible. Furthermore, this original one-pot method can be easily and widely used for many other diseases and target biomarkers by targeting-moiety introduced specific amphiphiles.

REFERENCE

1. Siegel R, Ma J, Zou Z, Jemal A. Cancer statistics, 2014. *CA Cancer J Clin.* 2014;64:9-29.
2. Ferlay J, Soerjomataram I, Dikshit R, et al. Cancer incidence and mortality worldwide: sources, methods and major patterns in GLOBOCAN 2012. *Int J Cancer.* 2015;136:E359-E386.
3. Eustatia-Rutten C, Smit J, Romijn J, et al. Diagnostic value of serum thyroglobulin measurements in the follow-up of differentiated thyroid carcinoma, a structured meta-analysis. *Clinical endocrinology.* 2004;61:61-74.
4. Jung K-W, Won Y-J, Kong H-J, et al. Cancer statistics in Korea: incidence, mortality, survival, and prevalence in 2012. *Cancer Res Treat.* 2015;47:127.
5. Stenman U-H, Leinonen J, Zhang W-M, Finne P. Prostate-specific antigen. Paper presented at: *Semin Cancer Biol.*, 1999.
6. Trover JK, Beckett ML, Wright GL. Detection and characterization of the prostate-specific membrane antigen (PSMA) in tissue extracts and body fluids. *Int J Cancer.* 1995;62:552-558.
7. Eder M, Eisenhut M, Babich J, Haberkorn U. PSMA as a target for radiolabelled small molecules. *Eur J Nucl Med Mol Imaging.* 2013;40:819-823.
8. Yu MK, Kim D, Lee IH, So JS, Jeong YY, Jon S. Image-Guided Prostate Cancer Therapy Using Aptamer-Functionalized Thermally

Cross-Linked Superparamagnetic Iron Oxide Nanoparticles. *Small.* 2011;7:2241-2249.

9. Kratochwil C, Giesel FL, Leotta K, et al. PMPA for nephroprotection in PSMA-targeted radionuclide therapy of prostate cancer. *J Nucl Med.* 2015:jnumed. 114.147181.

10. Chen Z, Penet M-F, Nimmagadda S, et al. PSMA-targeted theranostic nanoplex for prostate cancer therapy. *ACS nano.* 2012;6:7752-7762.

11. Schipper ML, Iyer G, Koh AL, et al. Particle size, surface coating, and PEGylation influence the biodistribution of quantum dots in living mice. *Small.* 2009;5:126-134.

12. Chen Y, Foss CA, Byun Y, et al. Radiohalogenated prostate-specific membrane antigen (PSMA)-based ureas as imaging agents for prostate cancer. *J Med Chem.* 2008;51:7933-7943.

13. Ristau BT, O'Keefe DS, Bacich DJ. The prostate-specific membrane antigen: lessons and current clinical implications from 20 years of research. *Urol Oncol.* 2014;32(3);272-9.

14. Afshar-Oromieh A, Malcher A, Eder M, et al. PET imaging with a [^{68}Ga] gallium-labelled PSMA ligand for the diagnosis of prostate cancer: biodistribution in humans and first evaluation of tumour lesions. *Eur J Nucl Med Mol Imaging.* 2013;40:486-495.

15. Nahrendorf M, Zhang H, Hembrador S, et al. Nanoparticle PET-CT imaging of macrophages in inflammatory atherosclerosis. *Circulation.* 2008;117:379-387.

16. Yan L, Zhang J, Lee CS, Chen X. Micro-and Nanotechnologies for Intracellular Delivery. *Small.* 2014;10:4487-4504.

17. Narayanan R, El-Sayed MA. Catalysis with transition metal nanoparticles in colloidal solution: nanoparticle shape dependence and stability. *J Phys Chem B.* 2005;109:12663-12676.

18. Knauert ST, Douglas JF, Starr FW. The effect of nanoparticle shape on polymer-nanocomposite rheology and tensile strength. *J Polym Sci B: Polym Phys.* 2007;45:1882-1897.

19. Li N, Binder WH. Click-chemistry for nanoparticle-modification. *J Mater Chem.* 2011;21:16717-16734.

20. Fang F, Zhao D, Li B, Zhang Z, Zhang J, Shen D. The enhancement of ZnO nanowalls photoconductivity induced by CdS nanoparticle modification. *Appl Phys Lett.* 2008;93:233115.

21. Lee YK, Jeong JM, Hoigebazar L, et al. Nanoparticles modified by encapsulation of ligands with a long alkyl chain to affect multispecific and multimodal imaging. *J Nucl Med.* 2012;53:1462-1470.

22. Yang BY, Moon S-H, Seelam SR, et al. Development of a multimodal imaging probe by encapsulating iron oxide nanoparticles with functionalized amphiphiles for lymph node imaging. *Nanomedicine (Lond).* 2015;10:1899-1910.

23. Lee DS, Im HJ, Lee YS. Radionanomedicine: Widened perspectives of molecular theragnosis. *Nanomedicine.* 2015;11:795-810.

24. Seo HJ, Nam SH, Im H-J, et al. Rapid Hepatobiliary Excretion of Micelle-Encapsulated/Radiolabeled Upconverting Nanoparticles as an Integrated Form. *Sci Rep.* 2015;5:15685.

25. Caravan P. Strategies for increasing the sensitivity of gadolinium based MRI contrast agents. *Chem Soc Rev.* 2006;35:512-523.

26. Hofmann M, Pichler B, Schölkopf B, Beyer T. Towards quantitative PET/MRI: a review of MR-based attenuation correction techniques. *Eur J Nucl Med Mol Imaging.* 2009;36:93-104.

27. Schulz V, Torres-Espallardo I, Renisch S, et al. Automatic, three-segment, MR-based attenuation correction for whole-body PET/MR data. *Eur J Nucl Med Mol Imaging.* 2011;38:138-152.

28. Zhou J, Yu M, Sun Y, et al. Fluorine-18-labeled Gd3þ/Yb3þ/Er3þ co-doped $NaYF_4$ nanophosphors for multimodality PET/MR/UCL imaging. *Biomaterials.* 2011;32:1148e1156.

29. Delso G, Fürst S, Jakoby B, et al. Performance measurements of the Siemens mMR integrated whole-body PET/MR scanner. *J Nucl Med.* 2011;52:1914-1922.

30. Aryal S, Key J, Stigliano C, Landis MD, Lee DY, Decuzzi P. Positron emitting magnetic nanoconstructs for PET/MR imaging. *Small.* 2014;10:2688-2696.

31. Schlyer D, Ravindranath B. Dual-Modality Preclinical PET/MRI Instrumentation. *Molecular Imaging of Small Animals*: Springer; 2014:409-445.

32. Drzezga A, Souvatzoglou M, Eiber M, et al. First clinical experience with integrated whole-body PET/MR: comparison to PET/CT in patients with oncologic diagnoses. *J Nucl Med.* 2012;53:845-855.

33. Kim JS, Kim Y-H, Kim JH, et al. Development and in vivo imaging of a PET/MRI nanoprobe with enhanced NIR fluorescence by dye encapsulation. *Nanomedicine (Lond).* 2012;7:219-229.

34. Lee H-Y, Li Z, Chen K, et al. PET/MRI dual-modality tumor imaging using arginine-glycine-aspartic (RGD)–conjugated radiolabeled iron oxide nanoparticles. *J Nucl Med.* 2008;49:1371-1379.

35. Thorek DL, Ulmert D, Diop N-FM, et al. Non-invasive mapping of deep-tissue lymph nodes in live animals using a multimodal PET/MRI nanoparticle. *Nat commun.* 2014;5.

36. Yang X, Hong H, Grailer JJ, et al. cRGD-functionalized, DOX-conjugated, and ^{64}Cu-labeled superparamagnetic iron oxide nanoparticles for targeted anticancer drug delivery and PET/MR imaging. *Biomaterials.* 2011;32:4151-4160.

37. Choi Js, Park JC, Nah H, et al. A hybrid nanoparticle probe for dual-modality positron emission tomography and magnetic resonance imaging. *Angew Chem Int Ed Engl.* 2008;47:6259-6262.

38. Tsoukalas C, Laurent G, Sánchez GJ, et al. Initial in vitro and in vivo assessment of Au@ DTDTPA-RGD nanoparticles for Gd-MRI and ^{68}Ga-PET dual modality imaging. *EJNMMI Phys.* 2015;2:A89.

39. Lewis CM, Graves SA, Hernandez R, et al. ^{52}Mn production for PET/MRI tracking of human stem cells expressing divalent metal transporter 1 (DMT1). *Theranostics.* 2015;5:227.

40. Binderup T, Lobatto M, Perez-Medina C, et al. PET/MRI to predict and quantify the uptake of ^{89}Zr-labeled nanoparticles in the aortic wall of atherosclerotic rabbits. *Paper presented at: Society of Nuclear Medicine Annual Meeting Abstracts,* 2014.

41. Tu C, Ng TS, Jacobs RE, Louie AY. Multimodality PET/MRI agents targeted to activated macrophages. *J Biol Inorg Chem.* 2014;19:247-258.

42. Truillet C, Lux F, Bouziotis P, et al. Development of ^{68}Ga/Gd^{3+} multimodal nanoparticles for PET/MRI dual imaging for tumor detection. *J Nucl Med.* 2015;56:273-273.

43. Zhernosekov KP, Filosofov DV, Baum RP, et al. Processing of generator-produced ^{68}Ga for medical application. *J Nucl Med.* 2007;48:1741-1748.

44. Meyer GJ, Macke H, Schuhmacher J, Knapp WH, Hofmann M. ^{68}Ga-labelled DOTA-derivatised peptide ligands. *Eur J Nucl Med Mol Imaging.* 2004;31:1097-1104.

45. Shetty D, Lee YS, Jeong JM. ^{68}Ga-labeled radiopharmaceuticals for positron emission tomography. *Nucl Med Mol Imaging.* 2010;44:233-240.

46. Jeong JM, Hong MK, Chang YS, et al. Preparation of a promising angiogenesis PET imaging agent: ^{68}Ga-labeled c(RGDyK)-

isothiocyanatobenzyl-1,4,7-triazacyclononane-1,4,7-triacetic acid and feasibility studies in mice. *J Nucl Med.* 2008;49:830-836.

47. Hoigebazar L, Jeong JM, Choi SY, et al. Synthesis and characterization of nitroimidazole derivatives for ^{68}Ga-labeling and testing in tumor xenografted mice. *J Med Chem.* 2010;53:6378-6385.

48. Breeman WA, de Blois E, Sze Chan H, Konijnenberg M, Kwekkeboom DJ, Krenning EP. ^{68}Ga-labeled DOTA-peptides and ^{68}Ga-labeled radiopharmaceuticals for positron emission tomography: current status of research, clinical applications, and future perspectives. *Semin Nucl Med.* 2011;41:314-321.

49. Babes L, Denizot Bt, Tanguy G, Le Jeune JJ, Jallet P. Synthesis of iron oxide nanoparticles used as MRI contrast agents: a parametric study. *J Colloid Interface Sci.* 1999;212:474-482.

50. Chertok B, Moffat BA, David AE, et al. Iron oxide nanoparticles as a drug delivery vehicle for MRI monitored magnetic targeting of brain tumors. *Biomaterials.* 2008;29:487-496.

51. Higuchi T, Anton M, Dumler K, et al. Combined reporter gene PET and iron oxide MRI for monitoring survival and localization of transplanted cells in the rat heart. *J Nucl Med.* 2009;50:1088-1094.

52. Rosen JE, Chan L, Shieh D-B, Gu FX. Iron oxide nanoparticles for targeted cancer imaging and diagnostics. *Nanomedicine.* 2012;8:275-290.

53. Schwarz S, Wong JE, Bornemann J, et al. Polyelectrolyte coating of iron oxide nanoparticles for MRI-based cell tracking. *Nanomedicine.* 2012;8:682-691.

54. Jon S, Lee H, Yu MK, Jeong YY. Multifunctional Superparamagnetic Iron Oxide Nanoparticles (SPION) for cancer imaging and therapy. *Nanomedicine.* 2007;3:348.

55. Xie J, Chen K, Huang J, et al. PET/NIRF/MRI triple functional iron oxide nanoparticles. *Biomaterials.* 2010;31:3016-3022.

56. Henry MD, Silva MD, Wen S, et al. Spiculated periosteal response induced by intraosseous injection of 22Rv1 prostate cancer cells resembles subset of bone metastases in prostate cancer patients. *The Prostate.* 2005;65:347-354.

57. Kovar JL, Cheung LL, Simpson MA, Olive DM. Pharmacokinetic and Biodistribution Assessment of a Near Infrared-Labeled PSMA-Specific Small Molecule in Tumor-Bearing Mice. *Prostate cancer.* 2014;2014.

58. Maresca K, Hillier S, Femia F, et al. A series of halogenated heterodimeric inhibitors of prostate specific membrane antigen (PSMA) as radiolabeled probes for targeting prostate cancer. *J Med Chem.* 2008;52:347-357.

59. Hillier SM, Kern AM, Maresca KP, et al. ^{123}I-MIP-1072, a small-molecule inhibitor of prostate-specific membrane antigen, is effective at monitoring tumor response to taxane therapy. *J Nucl Med.* 2011;52:1087-1093.

60. Cacheris WP, Quay SC, Rocklage SM. The relationship between thermodynamics and the toxicity of gadolinium complexes. *J Magn Reson Imaging.* 1990;8:467-481.

61. Maeda H. The enhanced permeability and retention (EPR) effect in tumor vasculature: the key role of tumor-selective macromolecular drug targeting. *Adv Enzyme Regul.* 2001;41:189-207.

62. Maeda H, Sawa T, Konno T. Mechanism of tumor-targeted delivery of macromolecular drugs, including the EPR effect in solid tumor and clinical overview of the prototype polymeric drug SMANCS. *J Control Release.* 2001;74:47-61.

63. Maeda H, Bharate G, Daruwalla J. Polymeric drugs for efficient tumor-targeted drug delivery based on EPR-effect. *Eur J Pharm Biopharm.* 2009;71:409-419.

64. Bergström M, Grahnen A, Långström B. Positron emission tomography microdosing: a new concept with application in tracer and early clinical drug development. *Eur J Clin Pharmacol.* 2003;59:357-366.

65. Yang BY. Development of a Multimodal Imaging Probe for Lymph Node Targeting Using Specific Amphiphile Encapsulation Technology on Iron Oxide Nanoparticles: *College of Medicine, Seoul National University*; 2014.

Appendix

Spectral Data

^{1}H-NMR

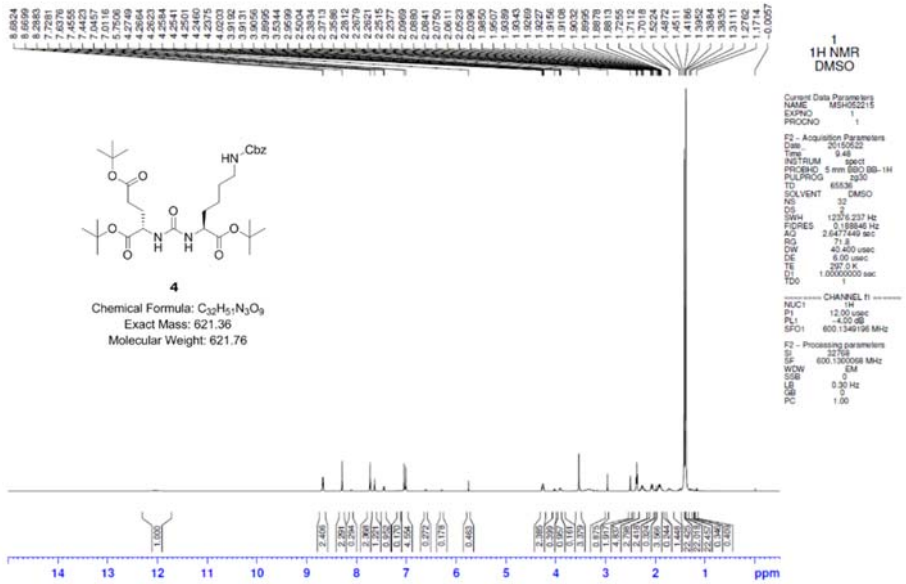
1
1H NMR
DMSO
HN
Cbz
4
Chemical Formula: C32H51N3O9
Exact Mass: 621.36
Molecular Weight: 621.76
ppm

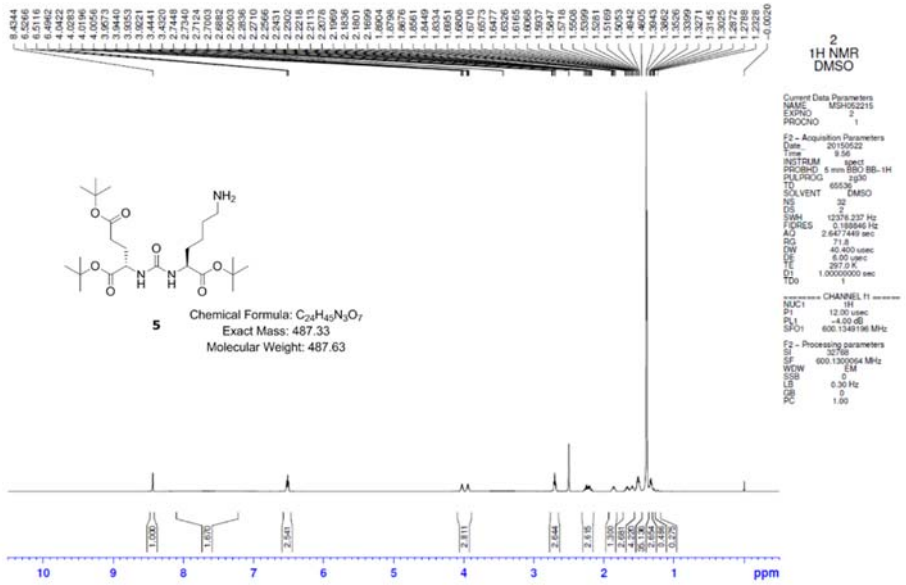
2
1H NMR
DMSO
NH2
5
Chemical Formula: C24H45N3O7
Exact Mass: 487.33
Molecular Weight: 487.63
ppm

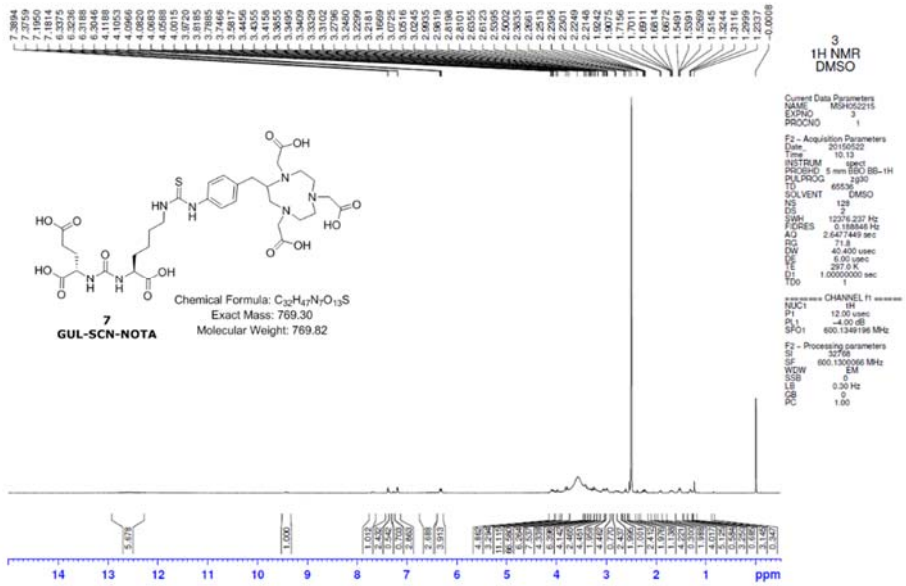
3
1H NMR
DMSO
Chemical Formula: C32H47N7O13S
Exact Mass: 769.30
Molecular Weight: 769.82
7
GUL-SCN-NOTA
ppm

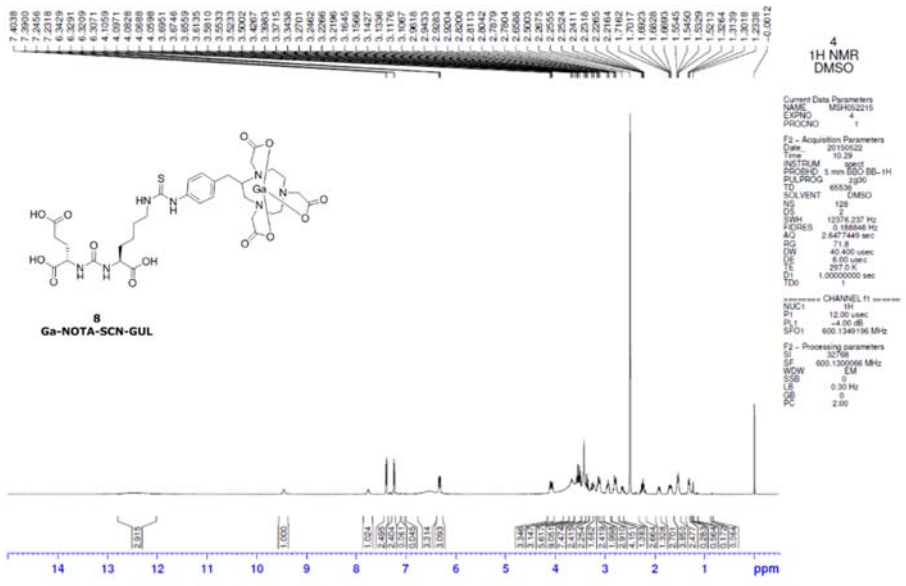
4
1H NMR
DMSO
8
Ga-NOTA-SCN-GUL
ppm

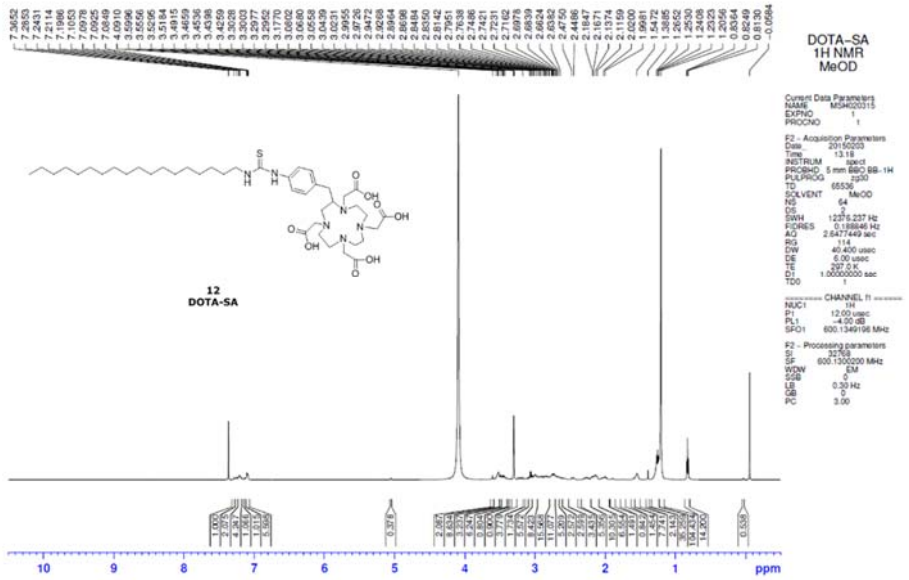
DOTA-SA
1H NMR
MeOD
12
DOTA-SA

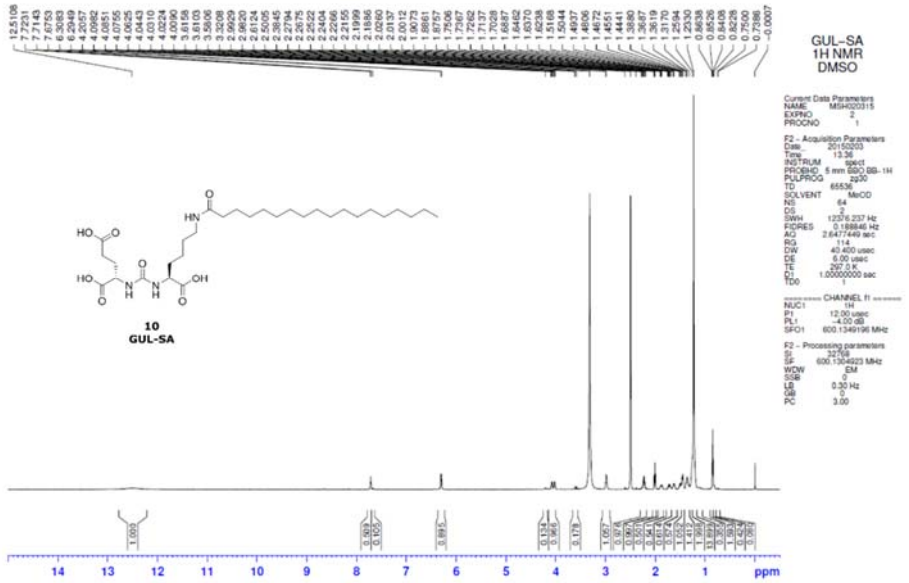
GUL-SA
1H NMR
DMSO
10
GUL-SA

Mass Spectra

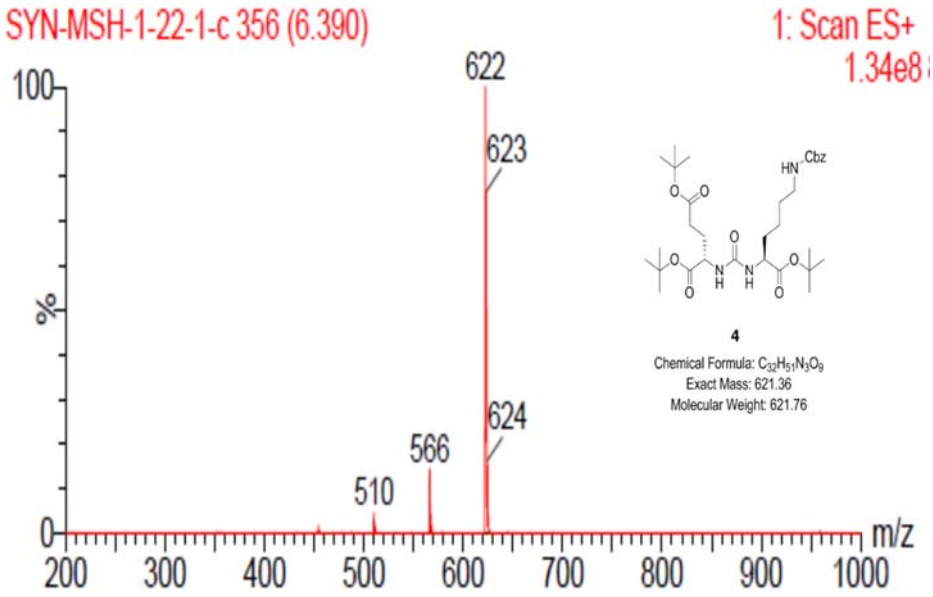
SYN-MSH-1-22-1-c 356 (6.390)
1: Scan ES+
1.34e8
100
%
0
622
623
624
566
510
200
300
400
500
600
700
800
900
1000
m/z
HN
Cbz
4
Chemical Formula: C32H51N3O9
Exact Mass: 621.36
Molecular Weight: 621.76

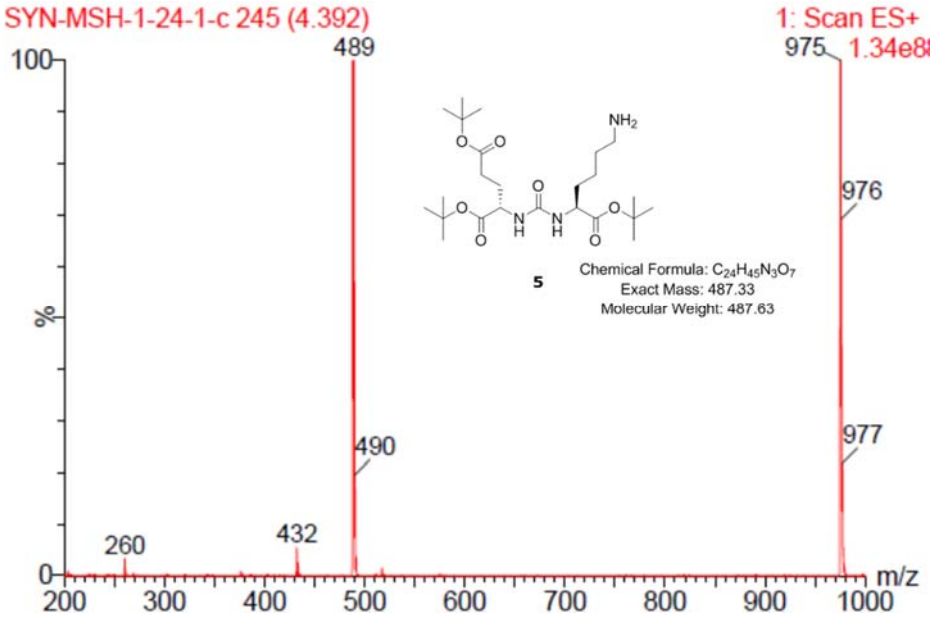
SYN-MSH-1-24-1-c 245 (4.392)
1: Scan ES+
1.34e8
100
%
0
489
490
260
432
975
976
977
200
300
400
500
600
700
800
900
1000
m/z
NH2
5
Chemical Formula: C24H45N3O7
Exact Mass: 487.33
Molecular Weight: 487.63

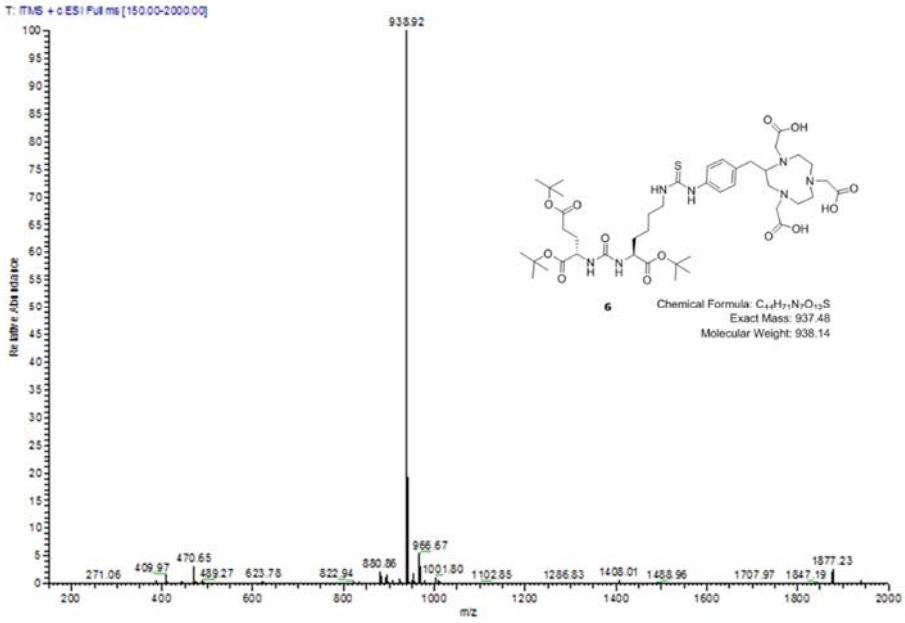
T: ITMS + c ESI Full ms [150.00-2000.00]
938.92
966.67
470.65
409.97
489.27
623.78
822.94
880.86
1001.80
1102.85
1286.83
1408.01
1488.96
1707.97
1847.19
1877.23
271.06
Relative Abundance
m/z
6
Chemical Formula: C44H71N7O13S
Exact Mass: 937.48
Molecular Weight: 938.14

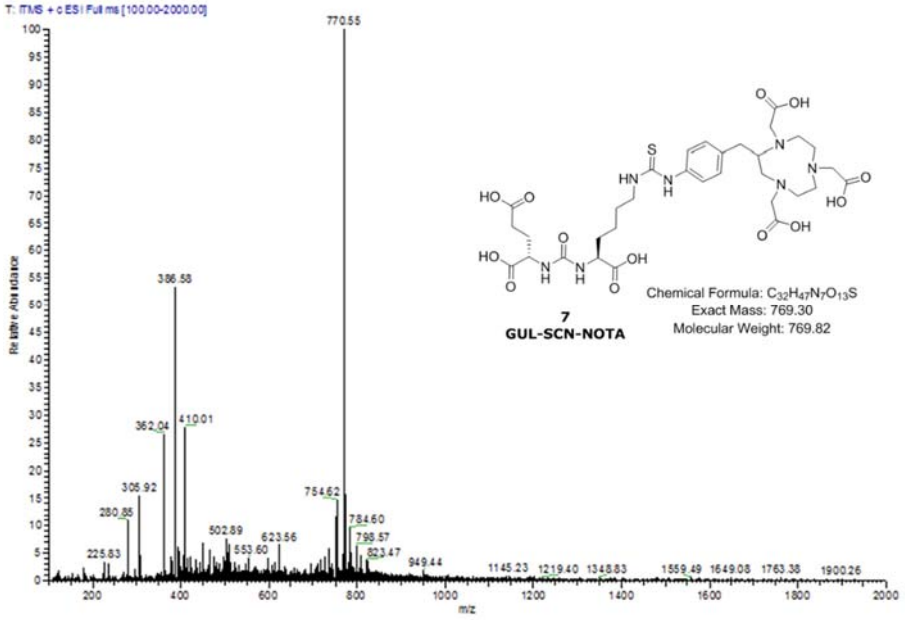
T: ITMS + c ESI Full ms [100.00-2000.00]
770.55
386.58
410.01
362.04
305.92
280.85
754.62
784.60
795.57
502.89
623.56
553.60
225.83
823.47
949.44
1145.23
1219.40
1348.83
1559.49
1649.08
1763.38
1900.26
Relative Abundance
m/z
7
GUL-SCN-NOTA
Chemical Formula: C32H47N7O13S
Exact Mass: 769.30
Molecular Weight: 769.82

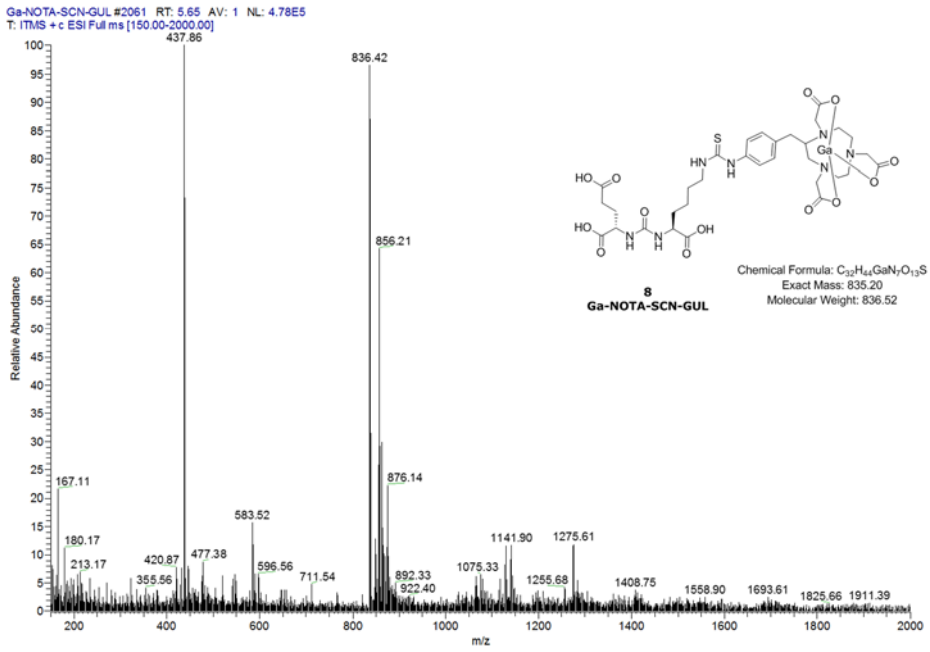
Ga-NOTA-SCN-GUL #2061 RT: 5.65 AV: 1 NL: 4.78E5
T: ITMS + c ESI Full ms [150.00-2000.00]
Relative Abundance
m/z
437.86
836.42
856.21
876.14
167.11
180.17
213.17
355.56
420.87
477.38
583.52
596.56
711.54
892.33
922.40
1075.33
1141.90
1255.68
1275.61
1408.75
1558.90
1693.61
1825.66
1911.39
8
Ga-NOTA-SCN-GUL
Chemical Formula: C32H44GaN7O13S
Exact Mass: 835.20
Molecular Weight: 836.52

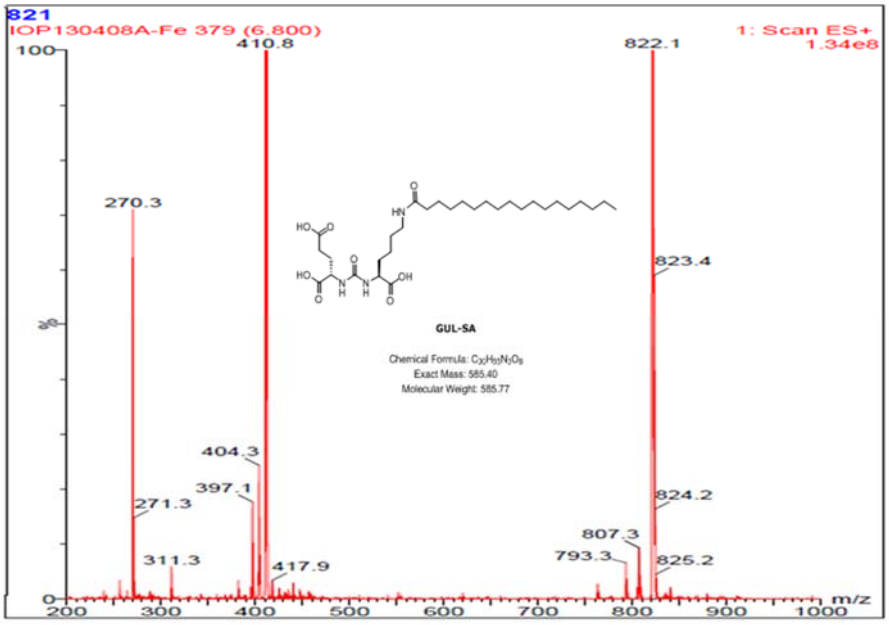
821
IOP130408A-Fe 379 (6.800)
1: Scan ES+
1.34e8
100
%
0
410.8
822.1
270.3
823.4
404.3
397.1
271.3
824.2
807.3
793.3
311.3
417.9
825.2
200
300
400
500
600
700
800
900
1000
m/z
GUL-SA
Chemical Formula: C32H59N3O8
Exact Mass: 585.40
Molecular Weight: 585.77

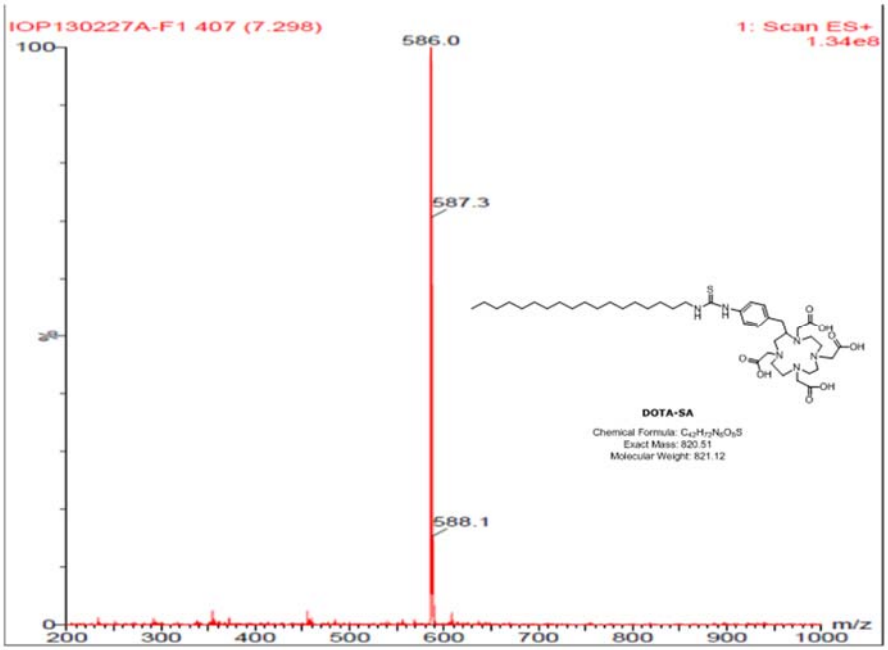
IOP130227A-F1 407 (7.298)
1: Scan ES+
1.34e8
100
%
0
586.0
587.3
588.1
200
300
400
500
600
700
800
900
1000
m/z
DOTA-SA
Chemical Formula: C40H72N6O7S
Exact Mass: 820.51
Molecular Weight: 821.12

요약(국문초록)

이 연구는 특정 양친매성 물질을 이용하여 단순하고 효율적인 캡슐화 방법을 통해 PET, MRI 영상 획득용 다중영상 프로브의 개발을 진행하였다. 또한 산화철 나노입자를 핵으로 하여 PEG, DOTA, 그리고 전립선특이막항원 (prostate-specific membrane antigen: PSMA)을 표적으로 하는 GUL, 세 종을 이용하여 수용액에서 캡슐화하였다. 만들어진 DOTA-IO-GUL 나노입자의 크기는 11.01 ± 1.54 nm 였다. DOTA-IO-GUL 은 방사성 동위원소인 ^{68}Ga 을 이용하여 높은 효율로 표지 하였다. DOTA-IO-GUL 의 생물학적 활성은 PSMA 양성 암종인 22Rv1 세포에서 ^{125}I 가 표지 된 MIP-1072 (PSMA-targeting agent) 와의 경쟁적 결합 연구를 통하여 확인하였다. 또한 PSMA 양성 세포종인 22Rv1 과 PSMA 음성 세포종인 PC-3 를 각각 양 쪽 허벅지에 투여한 종양 이식 동물을 이용하여 PET 및 MR 영상 실험을 진행하였다. 이 연구에서 Ga-68 을 표지 한 ^{68}Ga-DOTA-IO-GUL 이 양성 암종인 22Rv1 에 흡수되는 반면 PSMA 음성 세포 암종인 PC-3 에서는 흡수되지 않은 결과를 통하여 PSMA 에 선택적으로 흡수됨을 보여주었다. MRI 영상은 높은 해상도를 보였고, PET 영상은 정량 및 특이성도 확인할 수 있었다. 결론적으로 PET 과 MRI 각각에서 사용이 가능한 DOTA-IO-GUL 화합물은 또한 상보적인 PET/MR 기기에서까지 사용이 가능한 다중영상 프로브로서, PSMA 를 표적으로 하는

전립선암 표적 영상용 산화철 나노입자 개발을 완료하였다. 이상의 결과로부터 본 연구진이 개발한 나노입자 표면개질 방법의 재현성과 확장성 검증 또한 완료하였다.

주요어: 나노입자, 산화철, 나노입자 표면개질 방법, 양전자단층촬영영상, 자기공명영상, 양전자단층촬영/자기공명영상, 전립선암, 전립선특이막항원, 다중영상, 갈륨-68

학번: 2011-30624